

INFORMATION TO USERS

This reproduction was made from a copy of a document sent to us for microfilming. While the most advanced technology has been used to photograph and reproduce this document, the quality of the reproduction is heavily dependent upon the quality of the material submitted.

The following explanation of techniques is provided to help clarify markings or notations which may appear on this reproduction.

1. The sign or "target" for pages apparently lacking from the document photographed is "Missing Page(s)". If it was possible to obtain the missing page(s) or section, they are spliced into the film along with adjacent pages. This may have necessitated cutting through an image and duplicating adjacent pages to assure complete continuity.
2. When an image on the film is obliterated with a round black mark, it is an indication of either blurred copy because of movement during exposure, duplicate copy, or copyrighted materials that should not have been filmed. For blurred pages, a good image of the page can be found in the adjacent frame. If copyrighted materials were deleted, a target note will appear listing the pages in the adjacent frame.
3. When a map, drawing or chart, etc., is part of the material being photographed, a definite method of "sectioning" the material has been followed. It is customary to begin filming at the upper left hand corner of a large sheet and to continue from left to right in equal sections with small overlaps. If necessary, sectioning is continued again—beginning below the first row and continuing on until complete.
4. For illustrations that cannot be satisfactorily reproduced by xerographic means, photographic prints can be purchased at additional cost and inserted into your xerographic copy. These prints are available upon request from the Dissertations Customer Services Department.
5. Some pages in any document may have indistinct print. In all cases the best available copy has been filmed.

**University
Microfilms
International**

300 N. Zeeb Road
Ann Arbor, MI 48106



1329212

Pao, Hsueh-yuan

**ELECTROMAGNETIC SCATTERING FROM A BRANCH LINE IN A PARALLEL
PLATE WAVEGUIDE**

The University of Arizona

M.S. 1986

**University
Microfilms
International** 300 N. Zeeb Road, Ann Arbor, MI 48106

**ELECTROMAGNETIC SCATTERING FROM A BRANCH LINE
IN A PARALLEL PLATE WAVEGUIDE**

by
Hsueh-yuan Pao

**A Thesis Submitted to the Faculty of the
DEPARTMENT OF ELECTRICAL AND COMPUTER ENGINEERING
In Partial Fulfillment of the Requirements
For the Degree of
MASTER OF SCIENCE
In the Graduate College
THE UNIVERSITY OF ARIZONA**

1 9 8 6

STATEMENT BY AUTHOR


This thesis has been submitted in partial fulfillment of requirements for an advanced degree at The University of Arizona and is deposited in the University Library to be made available to borrowers under rules of the Library.

Brief quotations from this thesis are allowable without special permission, provided that accurate acknowledgment of source is made. Requests for permission for extended quotation from or reproduction of this manuscript in whole or in part may be granted by the head of the major department or the Dean of the Graduate College when in his or her judgement the proposed use of the material is in the interests of scholarship. In all other instances, however, permission must be obtained from the author.

SIGNED: Arthur Pico

APPROVAL BY THESIS DIRECTOR

This thesis has been approved on the date shown below:

 9/11/64

D. G. Dudley
Professor of Electrical Engineering

ACKNOWLEDGMENTS

I am deeply indebted to Professor Donald G. Dudley for his constant encouragement, unlimited patience, and invaluable consultation and guidance. Special thanks also go to Professor Shan-jie Zhang and Professor James R. Wait for their unhesitating academic support and discussions at various times during the course of this work. I would also like to give sincere thanks to Mr. Peter Edsall, Dr. Robert R. Weyker, Mr. Jeffery T. Williams, Professor J. B. Andersen, and Mr. Mikaya L. D. Lumori for their helpful suggestions. I feel I have been very fortunate to work in such a fine academic setting with such knowledgeable and dedicated people. Finally, I would like to thank my parents, Chia-shan and Feng-mi, and my wife, Ming-ming for their encouragement.

CONTENTS

	Page
LIST OF ILLUSTRATIONS	vi
LIST OF TABLES	ix
ABSTRACT	ix
1 INTRODUCTION	1
2 PROBLEM FORMULATION	5
2.1 Geometry of a Parallel Plate Waveguide	5
2.2 TM Mode Equations	7
2.3 Solution to TM Mode Equations	9
2.4 Green's Functions	12
2.5 Expressions for the Fields	15
2.6 Integral Equation	17
3 LOW FREQUENCY APPROXIMATION	19
4 SOLUTION BY METHOD OF MOMENTS	27
4.1 Singularities of Integral Equation	27
4.2 Formulations for Method of Moments	29
4.3 Improvement of Convergence	33
4.4 Reflection Coefficient by MOM	36
4.5 Numerical Results	39
5 TIME DOMAIN RESULTS	57
5.1 Fundamentals of Fourier Transform Method	57
5.2 Exciting Signal	59
5.3 Analysis of Transient Responses	63
5.4 Numerical Results	64
6 CONCLUSIONS AND RECOMMENDATIONS	75
REFERENCES	77

LIST OF ILLUSTRATIONS

Figure	Page	
2-1	Two parallel plates of infinite extent are bounded by the y-z planes at $x = 0$ and $x = a$. A branch line of width d and depth c has one open face at the $x = 0$ plane. The source is located to the left of the aperture. The electromagnetic wave is propagating in the $+z$ direction.	6
3-1	The amplitude of the reflection coefficient by the low frequency approximation as a function of ω/ω_c , where $a = 1.5$, $d/a = 1.333$, and $c/a = 4.666$. ($\omega_c = 6.28 \times 10^8$ radians/second)	24
3-2	The equivalent circuit for the transmission line model.	25
4-1	The sketch map of the distribution of the aperture field. n denotes the source point, and ℓ denotes the observation point. $\Delta = \frac{d}{N}$	31
4-2	The product of the amplitude of the aperture field distribution E_A and the width of the aperture d , with $a = 2$, $d/a = 0.044$, $c/a = 1.33$, $k = 0.706$, and $N = 10$	40
4-3	The product of the amplitude of the aperture field distribution E_A and the width of the aperture d , with $a = 2$, $d/a = 0.044$, $c/a = 1.33$, $k = 0.706$, and $N = 20$	41
4-4	The product of the amplitude of the aperture field distribution E_A and the width of the aperture d , with $a = 2$, $d/a = 0.044$, $c/a = 1.33$, $k = 0.706$, and $N = 30$	42
4-5	The product of the amplitude of the aperture field distribution E_A and the width of the aperture d , with $a = 2$, $d/a = 0.044$, $c/a = 1.33$, $k = 0.706$, and $N = 50$	43
4-6	The product of the amplitude of the aperture field distribution E_A and the width of the aperture d , with $a = 2$, $d/a = 0.044$, $c/a = 1.33$, $k = 0.706$, and $N = 100$	44
4-7	The amplitude of the reflection coefficient by MOM as a function of N , where $a = 2$, $d/a = 0.444$, $c/a = 1.554$, and $k = 0.706$	46

LIST OF ILLUSTRATIONS - continued

Figure	Page
4-8 The amplitude of the reflection coefficient by MOM as a function of c/λ , where $a = 2$, $d/a = 1.33$, and $k = 0.706$	47
4-9 The amplitude of the reflection coefficient by MOM as a function of d/λ , where $a = 2$, $c/a = 0.955$, and $k = 0.706$	49
4-10 The amplitude of the reflection coefficient by MOM as a function of ω/ω_c , where $a = 1.5$, $d/a = 1.166$, and $c/a = 4.666$. ($\omega_c = 6.28 \times 10^8$ radians/second)	50
4-11 The amplitude of the reflection coefficient by MOM as a function of ω/ω_c , where $a = 1.5$, $d/a = 0.666$, and $c/a = 4.666$. ($\omega_c = 6.28 \times 10^8$ radians/second)	51
4-12 The amplitude of the reflection coefficient by MOM as a function of ω/ω_c , where $a = 1.5$, $d/a = 1.5$, and $c/a = 4.666$. ($\omega_c = 6.28 \times 10^8$ radians/second)	53
4-13 The solid line denotes $ \Gamma $ by MOM as a function of ω/ω_c , the dashed line with \square denotes $ \Gamma $ using the low frequency approximation as a function of ω/ω_c , where $a = 1.5$, $d/a = 1.333$, and $c/a = 4.666$. ($\omega_c = 6.28 \times 10^8$ radians/second)	55
5-1 The double exponential pulse function with the parameters $\alpha = 1.0 \times 10^7$ and $\beta = 1.0 \times 10^8$	61
5-2 The spectral function of the double exponential function with the parameters $\alpha = 1.0 \times 10^7$ and $\beta = 1.0 \times 10^8$	62
5-3 The transient response of the reflection coefficient $g_r(\omega_c t)$, where $a = 1.5$, $d/a = 1.333$, and $c/a = 4.833$. ($\omega_c = 6.28 \times 10^8$ radians/second)	65
5-4 The transient response of the reflection coefficient $g_r(\omega_c t)$, where $a = 1.5$, $d/a = 1.333$, and $c/a = 24.0$. ($\omega_c = 6.28 \times 10^8$ radians/second)	66
5-5 The transient response of the reflection coefficient $g_r(\omega_c t)$, where $a = 1.5$, $d/a = 1.333$, and $c/a = 4.833$. ($\omega_c = 6.28 \times 10^8$ radians/second)	67
5-6 The transient response of the reflection coefficient $g_r(\omega_c t)$, where $a = 1.5$, $d/a = 2.666$, and $c/a = 4.833$. ($\omega_c = 6.28 \times 10^8$ radians/second)	68

LIST OF ILLUSTRATIONS - continued

Figure	Page
5-7 The transient response of the reflection coefficient $g_r(\omega_c t)$, where $a = 1.5$, $d/a = 0.833$, $c/a = 4.666$, rise time = $14.28ns$, and fall time = $134.12ns$. ($\omega_c = 6.28 \times 10^8$ radians/second)	70
5-8 The transient response of the reflection coefficient $g_r(\omega_c t)$, where $a = 1.5$, $d/a = 0.833$, $c/a = 4.666$, rise time = $41.8ns$, and fall time = $228ns$. ($\omega_c = 6.28 \times 10^8$ radians/second)	71
5-9 The solid line denotes $g_r(\omega_c t)$ with the parameters $a = 1.5$, $d/a = 1.333$, and $c/a = 4.833$. The dashed line with \square denotes $g_r(\omega_c t)$, with the parameters $a = 1.5$, $d/a = 1.333$, and $c/a = 10.0$. ($\omega_c = 6.28 \times 10^8$ radians/second)	73
5-10 The solid line denotes $g_r(\omega_c t)$ with the parameters $a = 1.5$, $d/a = 1.333$, and $c/a = 4.666$. The dashed line with \square denotes $g_r(\omega_c t)$, with the parameters $a = 1.5$, $d/a = 1.166$, and $c/a = 4.666$. ($\omega_c = 6.28 \times 10^8$ radians/second)	74

LIST OF TABLES

Table		Page
4-1	Number of terms of convergence for $\sum_{m=1}^{\infty} \frac{\sin mx}{m^2}$	37
4-2	Number of terms of convergence for $\sum_{m=1}^{\infty} \frac{e^{-mz}}{m^2}$	38

ABSTRACT

The transient fields that are scattered by a branch line in a parallel plate waveguide are presented. The scattered fields can be used to estimate the width and the depth of the branch line. We propose this simulation problem to obtain synthetic data for future use in parametric inverse experiments.

We employ the Fourier transformation method to solve this problem. In the frequency domain, the Green's function method is used to formulate the field equations everywhere in the structure. The boundary conditions are imposed at the aperture to establish an integral equation. The field at the aperture separating the waveguide and branch line is found by solving the integral equation using an approximation valid at low frequencies and the method of moments (MOM). The reflection coefficient is evaluated over a broad enough range of frequencies to make possible the inverse transformation to the time-domain using the inverse fast Fourier transform (IFFT). The numerical results in both the time domain and the frequency domain are presented and analyzed.

CHAPTER 1

INTRODUCTION

Strictly speaking, all electromagnetic phenomena are transient since it is impossible for an electromagnetic phenomenon to exist at a single steady frequency from $t = -\infty$ to $t = \infty$. In practice, the engineer's only requirement for steady state is that the signal generators and the microwave components related to these generators worked under a single steady frequency condition for a long period of time. Although the study of time-harmonic problems is often much easier than that of the transient state, there has been an increasing demand to deal with transient electromagnetic phenomena in modern scientific problems.

Transient electromagnetic problems arise typically in the study of electromagnetic remote sensing, shielding effectiveness, electromagnetic compatibility, radar target identification, and the electromagnetic effects generated by a nuclear blast or lightning. Several techniques have been used in determining the transient electromagnetic response of various systems. One traditional method is called the Fourier transform method. It finds the time-harmonic response of the system under consideration as a function of frequency. The time-domain solution is then obtained by performing an inverse Fourier transformation. Much has been written on the subject of the frequency domain solution of electromagnetic scattering and radiation problems using an integral equation technique when applied to time-domain signals (Mittra, 1973). Numerical methods are generally used in the frequency-domain solution for many different frequencies. The development of high-speed computers has

revolutionized the capability for solving transient electromagnetic field problems by Fourier inversion. In short, the Fourier transform method provides a physical picture in frequency-domain problems, which are very familiar now, to aid the study of transient problems. Since the development of high-speed computers and the invention of the fast Fourier transform (FFT), the Fourier transform method can be used to efficiently solve the transient problem in practice.

When geophysical explorations are made of underground deposits, for example, it is often necessary to know the depth, the width and the position of the crack where the deposits may be hidden. Sometimes such an underground structure may be simulated by a simple model, such as a parallel-plate waveguide with a branch line. This is an example where the study of the parallel-plate waveguide structure is of significance for parametric inverse experiments.

In this work, we use the Fourier transform approach to study the transient scattered fields in a parallel plate waveguide in which a branch line is joined at one side of the waveguide. This problem can be classified as a discontinuity problem in uniform waveguide. Much effort has been spent on this type of problem in the frequency domain. For example, Marcuvitz (1951) resolved the waveguide discontinuity problem into its equivalent network, where each waveguide geometry has its own characteristic equivalent circuit and graphical solutions. Auda and Harrington (1983) have developed a moment procedure to solve waveguide junction problems which uses the generalized network formulation for aperture problems. Glaser (1970) has used the finite difference Green's function approach for solving the time harmonic scattering of a TE_{10} mode impinging on cylindrical metal posts in rectangular waveguides. Lee, Jones, and Campbell (1971) have investigated the convergence of numerical solutions in iris-type discontinuity problems. Hill and

Wait (1980) analyzed the two-dimensional model of intersecting mine tunnels with walls of finite impedance using a three-region mode matching technique. All these studies have emphasized the study of the frequency domain in solving electromagnetic problems. Transient problems have been studied for some typical parallel plate waveguide problems (Dudley and Quintenz, 1972; Shen, King and Wu, 1983; King and Blejer, 1979). In addition, much time and effort has been spent in applying transient electromagnetic method to practical geophysical exploration problems (Wait, 1982). Other current work by Wait (1986) reviews and summarizes the basic theoretical research on the propagation of the electromagnetic pulse signal over the surface of the earth. Various topics are given in the bibliography. However, we have not seen any recent publications dealing with a problem similar to the one we are studying here.

The problem to be studied in this thesis is introduced in chapter 2. The TM mode equations are derived from Maxwell's equations, and the Green's function method (Stakgold, 1979) is invoked to find the fields in the structure. Based on the required boundary conditions, an integral equation for determining the aperture field is written. In chapter 3, we employ low frequency methods to solve the integral equation and give the expressions for the fields and the reflection coefficient by this approach. In chapter 4, the integral equation is converted into a matrix equation by method of moments (MOM). The methods used in evaluating the matrix elements are then discussed. The fields everywhere in the structure and the reflection coefficient are determined from the computed aperture field. Various numerical results are demonstrated. The results of MOM and the low frequency approach are compared. The discussions in this chapter are restricted to the frequency-domain. The time-domain responses are calculated in chapter 5 by the Fourier transform

method. Comments are given for the numerical results. General conclusions and recommendations for further work are included in chapter 6.

CHAPTER 2

PROBLEM FORMULATION

In this chapter, we first introduce the geometry of the problem, and the coordinate system to be used. Next, we review the procedure for determining the independent TM mode equations from Maxwell's equations, and specify the sources. We then formulate the expressions for the magnetic fields in the main waveguide and the branch line. We formulate the magnetic field in each region by invoking Green's theorem and applying the boundary conditions. We next solve for the Green's functions in both regions, and define the proper source in the main waveguide. Finally, we derive an integral equation for the aperture linking the two regions by imposing the boundary conditions and matching the field equations on each side of the aperture.

2.1 Geometry of a Parallel Plate Waveguide

The problem to be considered is shown in Fig. 2-1, where a perfectly conducting parallel plate waveguide is bounded by the y - z planes extending to infinity, at $x = 0$ and $x = a$. We choose Cartesian coordinates for our coordinate system. The bottom plate of the parallel plate waveguide is located at the $x = 0$ plane. A branch line of width d terminated by a shorting plate at depth c is located beneath the bottom plate. One side of the branch line is at the $z = 0$ plane. Both regions are air filled. The wave propagates in the main waveguide in the positive z direction. A magnetic current sheet source is located in the main waveguide to the left of the

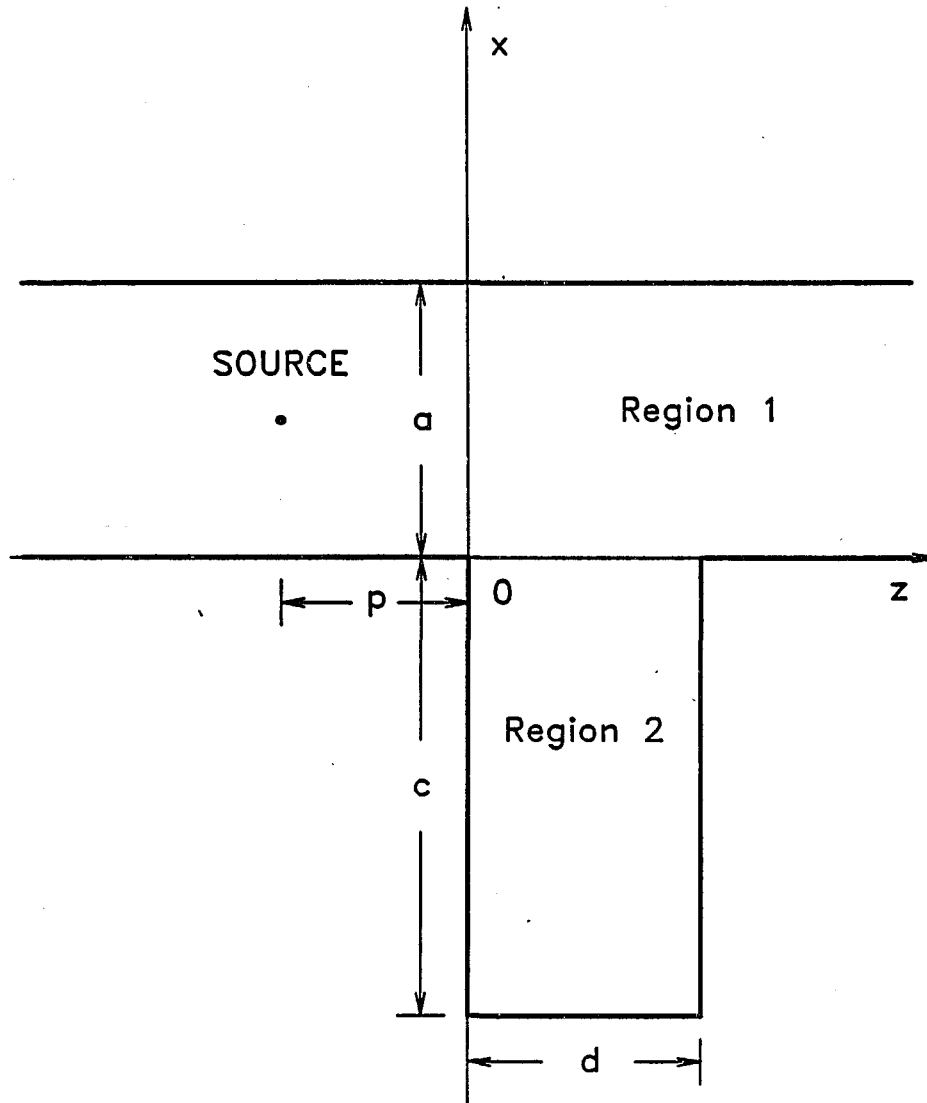


Figure 2-1 Two parallel plates of infinite extent are bounded by the y - z planes at $x = 0$ and $x = a$. A branch line of width d and depth c has one open face at the $x = 0$ plane. The source is located to the left of the aperture. The electromagnetic wave is propagating in the $+z$ direction.

branch line. The a -dimension is adjusted so that only the TEM wave is above cutoff in the main waveguide. Part of the incident wave will be scattered by the aperture. We wish to determine the fields back-scattered by the aperture as a function of time and space. Clearly our problem is two dimensional, since there is no variation in the y -direction.

2.2 TM Mode Equations

In this section we describe the TM mode solution for the parallel plate waveguide. This classical solution is the starting point for the solution of our problem. We first separate Maxwell's equations into two sets of equations: the TE and TM sets. Second, we derive the scalar Helmholtz wave equation for the TM modes. Finally, we specify the source that excites only the TM modes in the waveguide.

Maxwell's Equations in the frequency domain are given by

$$\nabla \times \vec{E} = -i\omega\mu\vec{H} - \vec{M} \quad (2-1)$$

$$\nabla \times \vec{H} = i\omega\epsilon\vec{E} + \vec{J} \quad (2-2)$$

where $\vec{M} = \vec{x}M_x + \vec{y}M_y + \vec{z}M_z$ and $\vec{J} = \vec{x}J_x + \vec{y}J_y + \vec{z}J_z$ are the magnetic and electric current density sources, respectively, and \vec{x} , \vec{y} , \vec{z} are the unit vectors in the x , y , z directions, respectively. In the above equations, $e^{i\omega t}$ time dependence is assumed.

Because the problem is independent of y -variation, we may set

$$\frac{\partial}{\partial y} = 0 \quad (2-3)$$

in (2-1) and (2-2). Equations (2-1) and (2-2) can be written in terms of Cartesian field components as follows:

$$-\frac{\partial E_y}{\partial z} = -i\omega\mu H_x - M_x \quad (2-4)$$

$$-\left(\frac{\partial E_z}{\partial x} - \frac{\partial E_x}{\partial z}\right) = -i\omega\mu H_y - M_y \quad (2-5)$$

$$\frac{\partial E_y}{\partial x} = -i\omega\mu H_z - M_z \quad (2-6)$$

$$-\frac{\partial H_y}{\partial z} = i\omega\epsilon E_x + J_x \quad (2-7)$$

$$\frac{\partial H_x}{\partial z} - \frac{\partial H_z}{\partial x} = i\omega\epsilon E_y + J_y \quad (2-8)$$

$$\frac{\partial H_y}{\partial x} = i\omega\epsilon E_z + J_z \quad (2-9)$$

Equations (2-4), (2-6) and (2-8) form an independent set, while (2-5), (2-7) and (2-9) form a second independent set of equations. The first set, consisting of E_y , H_x , H_z and sources J_y , M_x , M_z , is transverse electric (TE) to the direction of propagation. The second set, consisting of H_y , E_x , E_z , and sources M_y , J_x , J_z , is transverse magnetic (TM) to the direction of propagation.

In the present situation, where $\partial/\partial y = 0$, it is clear that the TM and TE fields are uncoupled. It would therefore be possible to excite one set independently of the other by an appropriate selection of sources \vec{J} and \vec{M} . Recall that we require that the only permissible mode propagating in the waveguide, prior to incidence upon the branch line, is the TEM mode. We consider, therefore, the TM mode set, which contains the TEM mode as a set member. To this end, we set all sources

equal to zero except M_y in equations (2-4) through (2-9). The result is that the TE equations are source-free and yield only the trivial solution.

To derive the TM mode equations, we differentiate equation (2-7) with respect to z and (2-9) with respect to x , and subtract to obtain:

$$\frac{\partial^2 H_y}{\partial x^2} + \frac{\partial^2 H_y}{\partial z^2} = i\omega\epsilon\left(\frac{\partial E_z}{\partial x} - \frac{\partial E_x}{\partial z}\right) \quad (2-10)$$

Substituting (2-5) into the bracket of the right hand side of (2-10), and grouping the source terms on the right hand side, we have the following TM mode equations:

$$\nabla_{xz}^2 H_y + k^2 H_y = i\omega\epsilon M_y = -f \quad (2-11)$$

$$E_x = -\frac{1}{i\omega\epsilon} \frac{\partial H_y}{\partial z} \quad (2-12)$$

$$E_z = \frac{1}{i\omega\epsilon} \frac{\partial H_y}{\partial x} \quad (2-13)$$

where

$$\nabla_{xz}^2 = \frac{\partial^2}{\partial x^2} + \frac{\partial^2}{\partial z^2} \quad (2-14)$$

2.3 Solution to TM Mode Equations

In this section, we formulate the expressions for the magnetic fields in the main waveguide and in the branch line. We do so by invoking Green's theorem and imposing the boundary conditions.

The TM mode equations are given in equations (2-11) through (2-13). We first take the inner product of (2-11) with a Green's function and then apply Green's theorem to obtain:

Region 1:

$$\begin{aligned}
\int_{R_1} g_1 f dx dz &= \int_{R_1} H_y [-(\nabla_{xz}^2 + k^2)] g_1 dx dz - \int_{-\infty}^{\infty} (H_y \frac{\partial g_1}{\partial x} - g_1 \frac{\partial H_y}{\partial x}) \Big|_{x=0} dz \\
&+ \int_{-\infty}^{\infty} (H_y \frac{\partial g_1}{\partial x} - g_1 \frac{\partial H_y}{\partial x}) \Big|_{x=a} dz + \int_0^a (H_y \frac{\partial g_1}{\partial z} - g_1 \frac{\partial H_y}{\partial z}) \Big|_{z=\infty} dx \\
&- \int_0^a (H_y \frac{\partial g_1}{\partial z} - g_1 \frac{\partial H_y}{\partial z}) \Big|_{z=-\infty} dx
\end{aligned} \tag{2-15}$$

Region 2:

$$\begin{aligned}
\int_{R_2} H_y [-(\nabla_{xz}^2 + k^2)] g_2 dx dz &- \int_0^d (H_y \frac{\partial g_2}{\partial x} - g_2 \frac{\partial H_y}{\partial x}) \Big|_{z=-c} dz \\
&+ \int_0^d (H_y \frac{\partial g_2}{\partial x} - g_2 \frac{\partial H_y}{\partial x}) \Big|_{x=0} dz + \int_0^{-c} (H_y \frac{\partial g_2}{\partial z} - g_2 \frac{\partial H_y}{\partial z}) \Big|_{z=d} dx \\
&- \int_0^{-c} (H_y \frac{\partial g_2}{\partial z} - g_2 \frac{\partial H_y}{\partial z}) \Big|_{z=0} dx = 0
\end{aligned} \tag{2-16}$$

where R_1 and R_2 indicate regions 1 and 2, respectively (Fig 2-1). Note that the assumption of y -independence causes the disappearance of integrations with respect to y in (2-15) and (2-16).

The components of \vec{E} tangential to the perfectly conducting surfaces are zero; in addition, \vec{H} vanishes as z approaches infinity since we assume a small loss in the medium in the waveguide; therefore, from equations (2-12) and (2-13) the normal components of the derivative of H_y are zero in equations (2-15) and (2-16), and $H_y = 0$ at $z = \pm\infty$.

The Green's function for this problem is chosen to satisfy

$$-(\nabla_{xz}^2 + k^2)g = \delta(x - x')(z - z') \tag{2-17}$$

and the following boundary conditions :

Region 1:

$$\frac{\partial H_y}{\partial x} \Big|_{x=0,a} = 0 \qquad \frac{\partial g_1}{\partial x} \Big|_{x=0,a} = 0 \qquad (2-18)$$

$$H_y \Big|_{z \rightarrow \pm\infty} = 0 \qquad g_1 \Big|_{z \rightarrow \pm\infty} = 0 \qquad (2-19)$$

Region 2:

$$\frac{\partial H_y}{\partial x} \Big|_{x=-c,0} = 0 \qquad \frac{\partial g_2}{\partial x} \Big|_{x=-c,0} = 0 \qquad (2-20)$$

$$\frac{\partial H_y}{\partial z} \Big|_{z=0,d} = 0 \qquad \frac{\partial g_2}{\partial z} \Big|_{z=0,d} = 0 \qquad (2-21)$$

By imposing the boundary conditions mentioned above and substituting the Green's function and the relationship $\partial H_y / \partial x = i\omega\epsilon E_z$ in equations (2-15) and (2-16), we obtain the magnetic field in the main waveguide as

$$H_{y1}(x, z) = \int_{R'_1} g_1 f dx' dz' - i\omega\epsilon \int_0^d g_1 E_{z1} \Big|_{x'=0} dz' \qquad (2-22)$$

and the magnetic field in the branch line as

$$H_{y2}(x, z) = i\omega\epsilon \int_0^d g_2 E_{z2} \Big|_{x'=0} dz' \qquad (2-23)$$

where H_{yi} and g_i are the magnetic fields and the Green's functions, respectively, and $i = 1, 2$ denotes the different regions.

2.4 Green's Functions

To complete the solutions for the fields, the Green's functions must be determined from the following differential equations and boundary conditions:

Region 1:

$$-(\nabla_{xx}^2 + k^2)g_1 = \delta(x - x')(z - z') \quad (2 - 24)$$

$$\left. \frac{\partial g_1}{\partial x} \right|_{x=0,a} = 0 \quad (2 - 25)$$

$$g_1 \Big|_{z \rightarrow \pm\infty} = 0 \quad (2 - 26)$$

Region 2:

$$-(\nabla_{xx}^2 + k^2)g_2 = \delta(x - x')(z - z') \quad (2 - 27)$$

$$\left. \frac{\partial g_2}{\partial x} \right|_{x=-c,0} = 0 \quad (2 - 28)$$

$$\left. \frac{\partial g_2}{\partial z} \right|_{z=0,d} = 0 \quad (2 - 29)$$

We begin by considering the solution in Region 1. The spectral expansion for the operator $-d^2/dx^2$ with Neumann boundary conditions is given by the Fourier cosine series (Friedman, 1956). We therefore expand g_1 as follows:

$$g_1 = \sum_{n=0}^{\infty} \sqrt{\frac{\epsilon_n}{a}} a_n(z) \cos \frac{n\pi x}{a} \quad (2 - 30)$$

where ϵ_n is the Neumann constant

$$\epsilon_n = \begin{cases} 1, & n = 0; \\ 2, & n \neq 0. \end{cases} \quad (2 - 31)$$

We substitute equation (2-30) into equation (2-24) and then take the inner product with the orthonormal function $\sqrt{\frac{\epsilon_m}{a}} \cos \frac{m\pi x}{a}$ producing the result

$$-\left(\frac{d^2}{dz^2} + k_z^2\right)a_m = \sqrt{\frac{\epsilon_m}{a}} \cos \frac{m\pi x'}{a} \delta(z - z') \quad (2-32)$$

where

$$k_z^2 = k^2 - \left(\frac{m\pi}{a}\right)^2 \quad (2-33)$$

We set

$$b_m = \frac{a_m}{\sqrt{\frac{\epsilon_m}{a}} \cos \frac{m\pi x'}{a}} \quad (2-34)$$

to give

$$-\left(\frac{d^2}{dz^2} + k_z^2\right)b_m = \delta(z - z') \quad (2-35)$$

From (2-26), the boundary condition for this eigenvalue problem is

$$b_m \Big|_{z \rightarrow \pm\infty} = 0 \quad (2-36)$$

Equations (2-35) and (2-36) form a standard Green's function problem. Following the conventional method by applying the continuity condition and the jump condition (Friedman, 1956) at $z = z'$, we obtain

$$b_m = \begin{cases} \frac{e^{-ik_z z'} e^{ik_z z}}{2ik_z}, & z < z'; \\ \frac{e^{ik_z z'} e^{-ik_z z}}{2ik_z}, & z > z'. \end{cases} \quad (2-37)$$

Substituting equation (2-37) into equations (2-34) and (2-30) yields

$$g_1(x, z | x', z') = \begin{cases} \sum_{m=0}^{\infty} \frac{\epsilon_m e^{ik_x(z-z')}}{a} \frac{1}{2ik_z} \cos \frac{m\pi x'}{a} \cos \frac{m\pi x}{a}, & z < z'; \\ \sum_{m=0}^{\infty} \frac{\epsilon_m e^{-ik_x(z-z')}}{a} \frac{1}{2ik_z} \cos \frac{m\pi x'}{a} \cos \frac{m\pi x}{a}, & z > z'. \end{cases} \quad (2-38)$$

where $\text{Im}(k_x) < 0$.

The procedure to solve g_2 is similar to the procedure to solve g_1 . We use the Fourier cosine spectral expansion for $-d^2/dx^2$ with Neumann boundary conditions to give

$$g_2 = \sum_{n=0}^{\infty} \sqrt{\frac{\epsilon_n}{d}} a_n(z) \cos \frac{n\pi z}{d} \quad (2-39)$$

After using a series of procedures which are similar to those for solving for g_1 , we obtain

$$b_m = \frac{a_m}{\sqrt{\frac{\epsilon_m}{d}} \cos \frac{m\pi z'}{d}} \quad (2-40)$$

and

$$-\left(\frac{d^2}{dx^2} + k_x^2\right)b_m = \delta(x - x') \quad (2-41)$$

where

$$k_x^2 = k^2 - \left(\frac{m\pi}{d}\right)^2 \quad (2-42)$$

The boundary condition for this eigenvalue problem is

$$\left.\frac{db_m}{dx}\right|_{x=0} = \left.\frac{db_m}{dx}\right|_{x=-c} = 0 \quad (2-43)$$

Following the same procedure as in the case for g_1 , we obtain

$$g_2(x, z | x', z') = \begin{cases} - \sum_{m=0}^{\infty} \frac{\epsilon_m \cos k_x(x' + c) \cos k_x x}{d k_x \sin k_x c} \cos \frac{m\pi z'}{d} \cos \frac{m\pi z}{d}, & x > x'; \\ - \sum_{m=0}^{\infty} \frac{\epsilon_m \cos k_x(x + c) \cos k_x x'}{d k_x \sin k_x c} \cos \frac{m\pi z'}{d} \cos \frac{m\pi z}{d}, & x < x'. \end{cases} \quad (2-44)$$

2.5 Expressions for the Fields

To produce an incoming TEM wave propagating in the positive z direction, we define the magnetic current source as follows:

$$M_y = \delta(z' + p) \quad (2-45)$$

where $p \geq 0$. Equation (2-45) states that the source is located on the left hand side (Fig 2-1) of the aperture, and is independent of x and y variation. We combine equations (2-11), (2-22) and (2-45) and perform the integral to obtain the source term. Note that the source point is always on the left hand side of the aperture; therefore, we use the expansion for g_1 , which is applicable wherever $z > z'$, in the source term. Since the source is x independent, the integral over x will vanish except when $m = 0$. This means that k_z degenerates to k and only the TEM wave survives.

After carrying out the integral over the source, we obtain $H_{y1}(x, z)$ for $z < 0$ as

$$H_{y1}(x, z) = -i\omega\epsilon \frac{e^{-ik(z+p)}}{2ik} - i\omega\epsilon \int_0^d \left[\frac{e^{ik(z-z')}}{2ika} + \sum_{m=1}^{\infty} \frac{e^{ik_x(z-z')}}{ik_z a} \cos \frac{m\pi x}{a} \right] E_{z1}(0, z') dz' \quad (2-46)$$

and $H_{y1}(x, z)$ for $z > d$ as

$$H_{y1}(x, z) = -i\omega\epsilon \frac{e^{-ik(z+p)}}{2ik} - i\omega\epsilon \int_0^d \left[\frac{e^{-ik(z-z')}}{2ika} + \sum_{m=1}^{\infty} \frac{e^{-ik_x(z-z')}}{ik_x a} \cos \frac{m\pi x}{a} \right] E_{z1}(0, z') dz' \quad (2-47)$$

and $H_{y1}(x, z)$ for $0 \leq z \leq d$ as

$$H_{y1}(x, z) = -i\omega\epsilon \frac{e^{-ik(z+p)}}{2ik} - i\omega\epsilon \left\{ \int_0^z \left[\frac{e^{-ik(z-z')}}{2ika} + \sum_{m=1}^{\infty} \frac{e^{-ik_x(z-z')}}{ik_x a} \cos \frac{m\pi x}{a} \right] E_{z1}(0, z') dz' + \int_z^d \left[\frac{e^{ik(z-z')}}{2ika} + \sum_{m=1}^{\infty} \frac{e^{ik_x(z-z')}}{ik_x a} \cos \frac{m\pi x}{a} \right] E_{z1}(0, z') dz' \right\} \quad (2-48)$$

The magnetic fields in Region 2 are as follows:

$$H_{y2}(x, z) = -i\omega\epsilon \int_0^d \left[\frac{\cos k(x+c)}{kd \sin kc} + \sum_{m=1}^{\infty} \frac{2 \cos k_x(x+c)}{k_x d \sin k_x c} \cos \frac{m\pi z'}{d} \cos \frac{m\pi z}{d} \right] E_{z2}(0, z') dz' \quad (2-49)$$

Equations (2-46) through (2-49) conclude the formulations for the magnetic fields in both regions. The only unknowns in these expressions are the aperture fields $E_{z1}(0, z')$ and $E_{z2}(0, z')$. Our task in the next section is to find these unknown fields.

2.6 Integral Equation

In order to find the aperture fields, we will match the fields in the main waveguide and in the branch line across the aperture by imposing the boundary conditions, and an integral equation will result. The integral equation is solved for the aperture field which can be used to find the field anywhere in the two regions.

We first find the magnetic fields in the aperture of both regions. This can be achieved by setting $x = 0$ in equations (2-48) and (2-49). The fields at the aperture can be written as:

$$\begin{aligned}
 H_{y1}(0, z) = & -i\omega\epsilon \frac{e^{-ik(z+p)}}{2ik} - i\omega\epsilon \left\{ \int_0^z \left[\frac{e^{-ik(z-z')}}{2ika} + \sum_{m=1}^{\infty} \frac{e^{-ik_x(z-z')}}{ik_x a} \right] E_{z1}(0, z') dz' \right. \\
 & \left. + \int_z^d \left[\frac{e^{ik(z-z')}}{2ika} + \sum_{m=1}^{\infty} \frac{e^{ik_x(z-z')}}{ik_x a} \right] E_{z1}(0, z') dz' \right\} \quad (2-50)
 \end{aligned}$$

$$\begin{aligned}
 H_{y2}(0, z) = & -i\omega\epsilon \int_0^d \left[\frac{\cot kc}{kd} + \sum_{m=1}^{\infty} \frac{2 \cot k_x c}{k_x d} \cos \frac{m\pi z'}{d} \cos \frac{m\pi z}{d} \right] E_{z2}(0, z') dz' \\
 & \quad (2-51)
 \end{aligned}$$

Let $H_{y1}(0, z) = H_{y2}(0, z)$ and $E_{z1}(0, z') = E_{z2}(0, z') = E_A(z')$ by the continuity of tangential electromagnetic fields at the aperture. We then obtain the following integral equation:

$$\begin{aligned}
 F = & -\frac{e^{-ik(z+p)}}{2ik} = \int_0^z \left[\frac{e^{-ik(z-z')}}{2ika} + \sum_{m=1}^{\infty} \frac{e^{-ik_x(z-z')}}{ik_x a} \right] E_A(z') dz' \\
 & + \int_z^d \left[\frac{e^{ik(z-z')}}{2ika} + \sum_{m=1}^{\infty} \frac{e^{ik_x(z-z')}}{ik_x a} \right] E_A(z') dz' \\
 & - \int_0^d \left[\frac{\cot kc}{kd} + \sum_{m=1}^{\infty} \frac{2 \cot k_x c}{k_x d} \cos \frac{m\pi z'}{d} \cos \frac{m\pi z}{d} \right] E_A(z') dz' \quad (2-52)
 \end{aligned}$$

In next two chapters, we will use two approaches to evaluate this equation. This will yield the aperture field $E_A(z')$ which can then be substituted into the field equations to obtain the complete solution set for the fields.

CHAPTER 3

LOW FREQUENCY APPROXIMATION

In this chapter, we propose to solve the integral equation (2-52) by a low frequency approximation. We will also derive the reflection coefficient in the main waveguide from the fields obtained by this approximation. Finally, a curve of the reflection coefficient will be drawn. The advantages of using the low frequency approximation are two fold. First, the integral equation reduces to an algebraic solution. Second, the reflection coefficient obtained can be used as a check on method of moments computations in the next chapter.

We start with the integral equation (2-52). It is well-known (Marcuvitz, 1951) that in the low frequency limit, calculations of field quantities away from the aperture become insensitive to the assumed form of the aperture field; therefore, we treat the aperture field $E_A(z')$ as a constant so that it can be taken out of the integral.

$$\begin{aligned}
 F(z) &= E_A \left[\int_0^z \frac{e^{-ik(z-z')}}{2ika} dz' + \int_z^d \frac{e^{ik(z-z')}}{2ika} dz' \right. \\
 &+ \int_0^z \sum_{m=1}^{\infty} \frac{e^{-ik_z(z-z')}}{ik_z a} dz' + \int_z^d \sum_{m=1}^{\infty} \frac{e^{ik_z(z-z')}}{ik_z a} dz' \\
 &\left. - \int_0^d \frac{\cot kc}{kd} dz' - \int_0^d \sum_{m=1}^{\infty} \frac{2 \cot k_x c}{k_x d} \cos \frac{m\pi z'}{d} \cos \frac{m\pi z}{d} dz' \right] \\
 &= E_A \left[\frac{e^{-ikz} + e^{ik(z-d)} - 2 - 2ak \cot kc}{2ak^2} \right]
 \end{aligned}$$

$$+ \sum_{m=1}^{\infty} \frac{e^{-ik_x z} + e^{ik_x(z-d)} - 2}{k_z^2 a} \quad (3-1)$$

We set the observation point in the middle of the aperture, i.e. $z = d/2$, then

$$F\left(\frac{d}{2}\right) = E_A \left[M\left(\frac{d}{2}\right) + \Delta\left(\frac{d}{2}\right) \right] \quad (3-2)$$

where

$$M\left(\frac{d}{2}\right) = \frac{e^{-ik_x \frac{d}{2}} - 1 - ak \cot kc}{ak^2} \quad (3-3)$$

$$\Delta\left(\frac{d}{2}\right) = \sum_{m=1}^{\infty} 2 \frac{e^{-ik_x \frac{d}{2}} - 1}{ak_z^2} \quad (3-4)$$

In (3-2), M is the TEM contribution, while Δ is the contribution from the higher order modes. We shall derive a condition under which the TEM contribution dominates in the integral equation.

Recall in last chapter that $\text{Im}(k_z) < 0$. For the low frequency case,

$$k \ll \frac{m\pi}{a} \quad (3-5)$$

therefore,

$$k_z \approx -i \frac{m\pi}{a} \quad (3-6)$$

also

$$k_z \approx -i \frac{m\pi}{d} \quad (3-7)$$

Substituting (3-6) into (3-4), we have

$$\Delta\left(\frac{d}{2}\right) \approx \sum_{m=1}^{\infty} 2a \frac{1 - e^{-\frac{m\pi d}{2a}}}{m^2 \pi^2} \quad (3-8)$$

We will try to find the upper bound of $\Delta(d/2)$. Since

$$\frac{e^{-\frac{m\pi d}{2a}}}{m^2\pi^2} > 0 \quad (3-9)$$

thus

$$\left| \Delta\left(\frac{d}{2}\right) \right| = \left| \sum_{m=1}^{\infty} 2a \frac{1 - e^{-\frac{m\pi d}{2a}}}{m^2\pi^2} \right| < \sum_{m=1}^{\infty} \frac{2a}{m^2\pi^2} = \frac{a}{3} \quad (3-10)$$

where we used the result (Collin, 1960)

$$\sum_{m=1}^{\infty} \frac{1}{m^2} = \frac{\pi^2}{6} \quad (3-11)$$

Note that for frequencies low enough,

$$M\left(\frac{d}{2}\right) = -\frac{\cot kc}{k} = \frac{\cos kc}{k \sin kc} \approx \frac{1}{k \cdot kc} \quad (3-12)$$

Comparing (3-10) and (3-12), we see that M dominates Δ so long as

$$ka \cdot kc \ll 3 \quad (3-13)$$

Therefore, we can eliminate all terms except the $m = 0$ term in the low frequency approximation so long as (3-13) is valid. The assumption that E_A is a constant and the neglect of the higher order modes leads us to an integral equation that can be solved analytically. The solution can be obtained in closed form as follows:

$$E_A = -ak \frac{e^{-ik(\frac{d}{2}+p)}}{2i \left(e^{-ik\frac{d}{2}} - 1 - ak \cot kc \right)} \quad (3-14)$$

The reflection coefficient is defined as the ratio of the reflected voltage to the incident voltage according to transmission line theory. In our problem, only the TEM wave can propagate along the main waveguide; therefore, we eliminate all higher modes in the field expressions. This can be achieved in practice by properly adjusting the width of the waveguide with respect to the wavelength.

We substitute equation (3-14) into (2-46) to obtain the magnetic field for $-p < x < 0$, viz:

$$H_{y1} = -i\omega\epsilon \frac{e^{-ik(z+p)}}{2ik} - i\omega\epsilon E_A \frac{e^{ikz}(e^{-ikd} - 1)}{2k^2 a} \quad (3-15)$$

The x -component of the electrical field is

$$\begin{aligned} E_x &= -\frac{1}{i\omega\epsilon} \frac{\partial H_y}{\partial z} \\ &= -\frac{e^{-ik(z+p)}}{2} + iE_A \frac{e^{ikz}(e^{-ikd} - 1)}{2ka} \end{aligned} \quad (3-16)$$

The voltage is found by integrating E_x across the waveguide to give

$$V = -a \frac{e^{-ik(z+p)}}{2} + iE_A \frac{e^{ikz}(e^{-ikd} - 1)}{2k} \quad (3-17)$$

The first term on the right hand side of equation (3-17) corresponds to the incident voltage and the second term corresponds to the reflected voltage. After substituting the aperture field E_A into equation (3-17), we find the reflection coefficient as follows:

$$\Gamma(\omega) = \frac{e^{i2kz}(e^{-ikd} - 1)e^{-ik\frac{d}{2}}}{2 \left(e^{-ik\frac{d}{2}} - 1 - ak \cot kc \right)} \quad (3-18)$$

The curve of the reflection coefficient as a function of the normalized frequency ω/ω_c is shown in Fig 3-1 with the parameters $a = 1.5$, $d/a = 1.333$, and $c/a = 4.666$, where ω_c is the first higher mode cutoff frequency in the main waveguide. When we draw the curve we set $z = 0$ in equation (3-18). This simply changes the time reference when we analyse the transient response of the reflection coefficient in chapter 5. Also we set

$$k = \frac{2\pi}{\lambda} = R \frac{2\pi}{\lambda_c} = R \frac{2\pi}{2a} = R \frac{\pi}{a} \quad (3-19)$$

in equation (3-18) for computing convenience, where R is a parameter ($0 \leq R \leq 1$), and $\lambda_c = 2a$ is the first cutoff wavelength in the main waveguide (Shen and Kong, 1983). Although the low frequency approach can not be used in general, it is a simple tool for checking the results of other approaches and can be utilized to find the fields in low frequency cases.

It is interesting to compare our result in (3-18) with what would be obtained in a simple transmission line model. According to transmission line theory, our geometry (Fig 2-1) can be represented by a simple equivalent circuit (Fig 3-2). The reflection coefficient Γ_T for the equivalent circuit is given by

$$\Gamma_T = \frac{z_{in} - z_0}{z_{in} + z_0} = \frac{z_s}{2z_0 + z_s} \quad (3-20)$$

where z_0 models the main line for $z > d$ and z_s models the branch line terminated by a short at $x = -c$. In our case, we easily find from transmission line analysis that

$$\Gamma_T = \frac{id}{2a \cot kc + id} \quad (3-21)$$

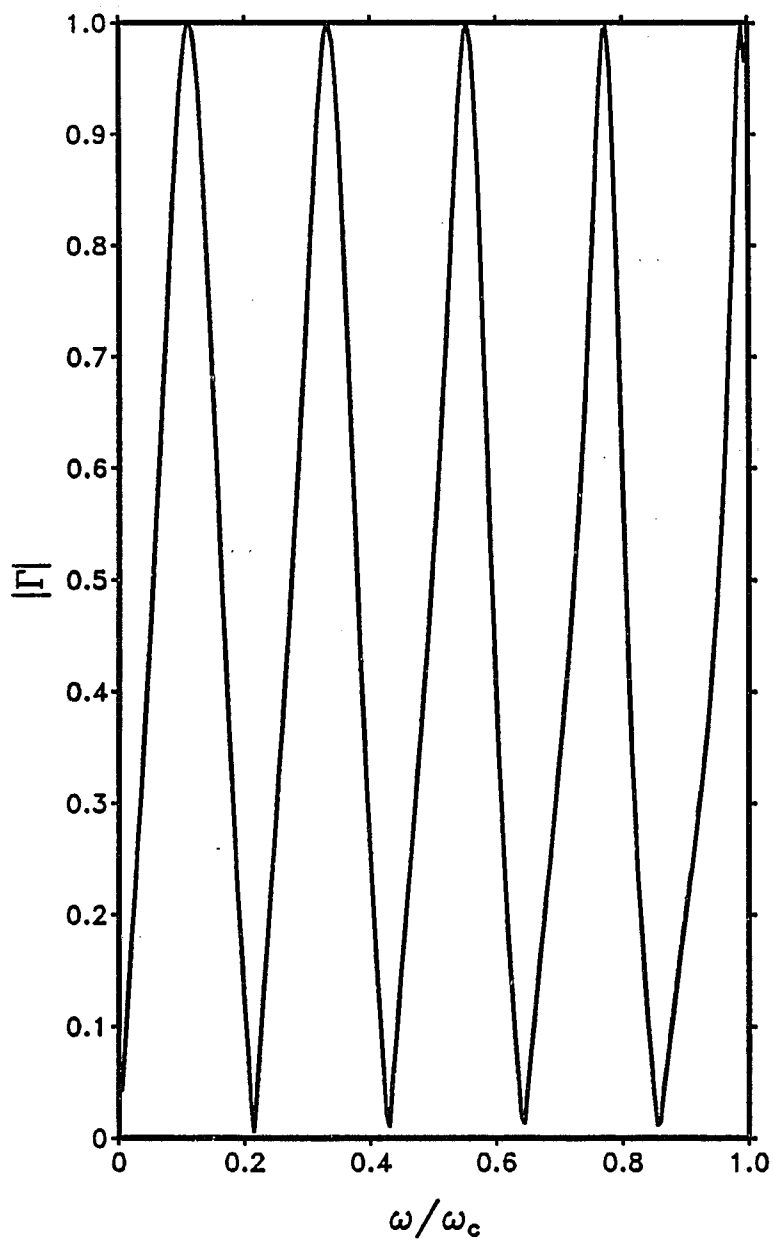


Figure 3-1 The amplitude of the reflection coefficient by the low frequency approximation as a function of ω/ω_c , where $a = 1.5$, $d/a = 1.333$, and $c/a = 4.666$. ($\omega_c = 6.28 \times 10^8$ radians/second)

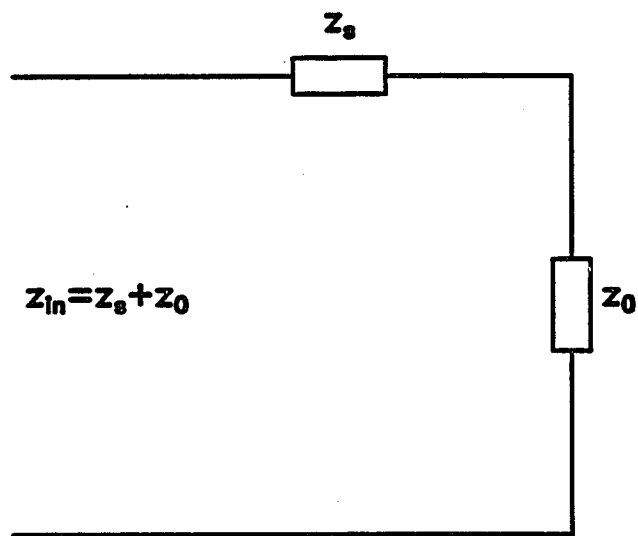


Figure 3-2 The equivalent circuit for the transmission line model.

If we use small argument approximations to the exponentials in (3-18),

$$\Gamma \longrightarrow \Gamma_T \quad (3-22)$$

CHAPTER 4

SOLUTION BY METHOD OF MOMENTS

In the last chapter, we solved the integral equation approximately by a method valid at low frequencies. We also found the reflection coefficient. All results obtained in the last chapter can only be applied to low frequency cases. In general, it is necessary to solve equation (2-52) numerically since the analytic solution to this problem does not exist in closed form. In this chapter, the method of moments (MOM) will be used to solve the integral equation. Before solving, the singularities of the integral equation will be investigated. It is important to properly select the expansion function and point testing function when using MOM. The reasons for selecting the pulse function as the expansion function and the impulse function as the point testing function will be explained. Some effort will be made to speed the calculation of the matrix elements as well. The reflection coefficient will be derived after the aperture field is found and compared to the low frequency result. Finally, the numerical results will be presented and discussed.

4.1 Singularities of Integral Equation

To find the solution of the integral equation by MOM, it is necessary to investigate the characteristics of the integral equation and discuss the singularities. In this section, we shall investigate the singularities of the integral equation (2-52) for further calculations.

Note that as $m \rightarrow \infty$,

$$k_z = \sqrt{k^2 - \left(\frac{m\pi}{a}\right)^2} \rightarrow -i\frac{m\pi}{a}, \quad (4-1)$$

$$k_x = \sqrt{k^2 - \left(\frac{m\pi}{d}\right)^2} \rightarrow -i\frac{m\pi}{d}, \quad (4-2)$$

and

$$\cot k_x c \rightarrow i. \quad (4-3)$$

Also

$$\frac{e^{-ik_x|z-z'|}}{ik_x a} \rightarrow \frac{e^{-\frac{m\pi}{a}|z-z'|}}{m\pi}, \quad (4-4)$$

and

$$\frac{\cot k_x c}{k_x d} \rightarrow -\frac{1}{m\pi}. \quad (4-5)$$

Subtracting and adding the asymptotic terms mentioned above, the integral equation (2-52) can be rewritten as:

$$\begin{aligned} F = \int_0^d \left\{ \frac{e^{-ik|z-z'|}}{2ika} - \frac{\cot kc}{kd} + \sum_{m=1}^{\infty} \left[\frac{e^{-ik_x|z-z'|}}{ik_x a} - \frac{e^{-\frac{m\pi}{a}|z-z'|}}{m\pi} \right] + S_1 \right. \\ \left. - \sum_{m=1}^{\infty} \left[\frac{2 \cot k_x c}{k_x d} + \frac{2}{m\pi} \right] \cos \frac{m\pi z'}{d} \cos \frac{m\pi z}{d} + S_2 \right\} E_A(z') dz' \quad (4-6) \end{aligned}$$

where

$$S_1 = \sum_{m=1}^{\infty} \frac{e^{-\frac{m\pi}{a}|z-z'|}}{m\pi} = \frac{1}{\pi} \ln \left| 1 - e^{-\frac{\pi}{a}|z-z'|} \right| \quad (4-7)$$

and

$$\begin{aligned}
 S_2 &= \sum_{m=1}^{\infty} \frac{2}{m\pi} \cos \frac{m\pi z'}{d} \cos \frac{m\pi z}{d} \\
 &= -\frac{1}{\pi} \left[\ln 4 + \ln \left| \sin \frac{\pi}{2d} (z + z') \right| + \ln \left| \sin \frac{\pi}{2d} (z - z') \right| \right] \quad (4-8)
 \end{aligned}$$

When z approaches z' , both S_1 and S_2 have a logarithmic singularity. Consequently, equation (2-52) has a logarithmic singularity.

There is also a spatial singularity at $z = 0$ and $z = d$ due to the edges of the waveguide. If the permittivities are the same in the main waveguide and in the branch line, the singularities behave approximately as $[z(z-d)]^{-\frac{1}{3}}$. (Jackson, 1975; Mittra and Lee, 1971; Andersen, 1978).

The singularities mentioned above will cause problems when solving the integral equation. In the next section, we will discuss the method for solving the integral equation that circumvents these singular problems.

4.2 Formulations for Method of Moments

The method of moments (MOM) is one of the important numerical methods used to solve differential and integral equations numerically (Harrington, 1968). MOM converts the differential or integral equation to a matrix equation by proper choice of the expansion function and the point testing function. The matrix function is then solved by known computational techniques. MOM also permits treatment of problems not solvable by exact methods. In our problem, we use collocation (Harrington, 1968); that is, the pulse function and impulse function are chosen as the expansion function and the testing function, respectively.

We divide the aperture into N intervals of equal width. Over the n th interval a pulse function can be described as follows:

$$P_n(z') = \begin{cases} 1, & (n-1)\frac{d}{N} \leq z' \leq n\frac{d}{N}; \\ 0, & \text{otherwise.} \end{cases} \quad (4-9)$$

The testing function $W_\ell(z)$ is located at the center of every interval; it is expressed as

$$W_\ell(z) = \delta \left[z - \frac{(2\ell-1)d}{2N} \right] \quad (4-10)$$

We approximate the aperture field by (Fig 4-1)

$$E_A(z') \approx \sum_{n=1}^N \alpha_n P_n(z') \quad (4-11)$$

After substituting equation (4-11) into (2-52), we take the inner product of both sides of equation (2-52) with the testing function $W_\ell(z)$ and obtain the following matrix equation:

$$[A_{\ell n}][\alpha_n] = [F_\ell] \quad (4-12)$$

where $\ell = 1, 2, \dots, N$, and $n = 1, 2, \dots, N$. For nondiagonal elements ($\ell > n$),

$$A_{\ell n} = \int_{\frac{(n-1)d}{N}}^{\frac{nd}{N}} \left\{ \frac{e^{-ik \left[\frac{(2\ell-1)d}{2N} - z' \right]}}{2ika} + \sum_{m=1}^{\infty} \frac{e^{-ik_x \left[\frac{(2\ell-1)d}{2N} - z' \right]}}{iak_x} \right\} dz' \\ - \int_{\frac{(n-1)d}{N}}^{\frac{nd}{N}} \left[\frac{\cot kc}{kd} + \sum_{m=1}^{\infty} \frac{2 \cot k_x c}{k_x d} \cos \frac{m\pi}{2N} (2\ell-1) \cos \frac{m\pi z'}{d} \right] dz' \quad (4-13)$$

In our case, the matrix is symmetric; therefore,

$$A_{n\ell} = A_{\ell n} \quad (4-14)$$

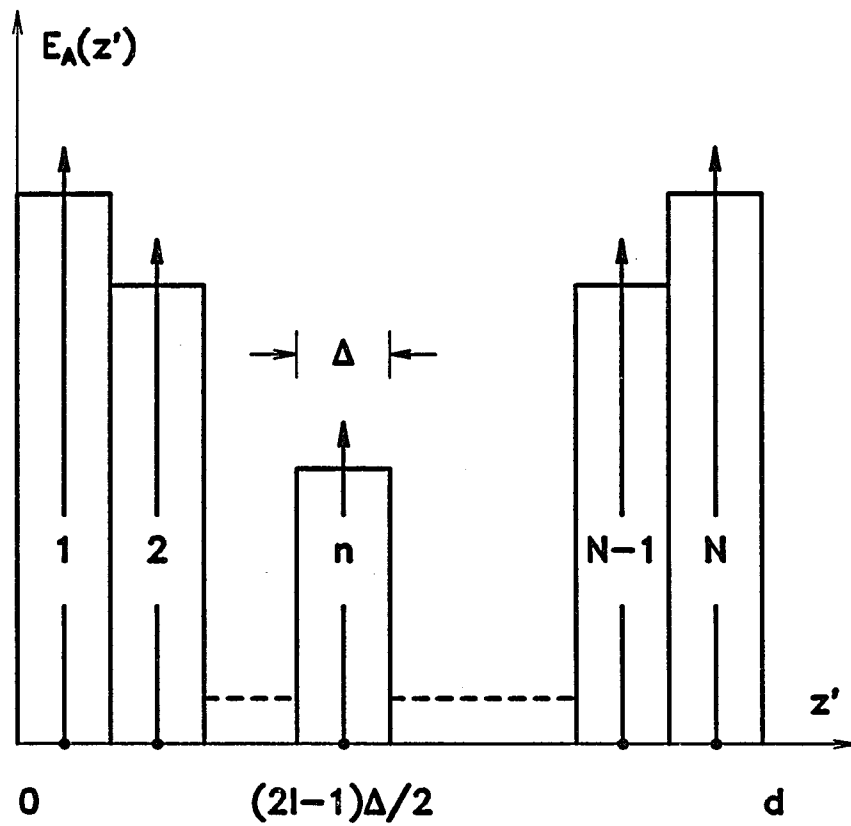


Figure 4-1 The sketch map of the distribution of the aperture field. n denotes the source point, and l denotes the observation point. $\Delta = \frac{d}{N}$.

For diagonal elements, ($\ell = n$)

$$\begin{aligned}
A_{\ell\ell} = & \int_{\frac{(n-1)d}{N}}^{\frac{(2\ell-1)d}{2N}-\epsilon} \left\{ \frac{e^{-ik\left[\frac{(2\ell-1)d}{2N}-z'\right]}}{2ika} + \sum_{m=1}^{\infty} \frac{e^{-ik_x\left[\frac{(2\ell-1)d}{2N}-z'\right]}}{iak_x} \right. \\
& - \frac{\cot kc}{kd} - \sum_{m=1}^{\infty} \frac{2 \cot k_x c}{k_x d} \cos \frac{m\pi}{2N} (2\ell-1) \cos \frac{m\pi z'}{d} \left. \right\} dz' \\
& + \int_{\frac{(2\ell-1)d}{2N}+\epsilon}^{\frac{\ell d}{N}} \left\{ \frac{e^{ik\left[\frac{(2\ell-1)d}{2N}-z'\right]}}{2ika} + \sum_{m=1}^{\infty} \frac{e^{ik_x\left[\frac{(2\ell-1)d}{2N}-z'\right]}}{iak_x} \right. \\
& - \frac{\cot kc}{kd} - \sum_{m=1}^{\infty} \frac{2 \cot k_x c}{k_x d} \cos \frac{m\pi}{2N} (2\ell-1) \cos \frac{m\pi z'}{d} \left. \right\} dz' \quad (4-15)
\end{aligned}$$

Finally, the elements of the source column vector are

$$F_{\ell} = -\frac{1}{2ik} e^{-ik\left[\frac{(2\ell-1)d}{2N}+p\right]} \quad (4-16)$$

It is clear from equation (4-10) that the observation point z approaches 0 and d but never arrives at these limits until N approaches infinity. Thus, in any numerical approximation, the edge singularities are avoided. Performing the integration in (4-13), we obtain

$$\begin{aligned}
A_{\ell n} = & \frac{e^{-ik\Delta(2\ell-2n+1)} - e^{-ik\Delta(2\ell-2n-1)}}{2k^2 a} + \sum_{m=1}^{\infty} \frac{e^{-ik_x\Delta(2\ell-2n+1)} - e^{-ik_x\Delta(2\ell-2n-1)}}{k_x^2 a} \\
& - \frac{\cot kc}{kN} - \sum_{m=1}^{\infty} \frac{2 \cot k_x c}{k_x m\pi} \left[\sin \frac{m\pi}{2N} (2\ell+2n-1) - \sin \frac{m\pi}{2N} (2\ell+2n-3) \right. \\
& \left. - \sin \frac{m\pi}{2N} (2\ell-2n-1) + \sin \frac{m\pi}{2N} (2\ell-2n+1) \right] \quad (4-17)
\end{aligned}$$

where

$$\Delta = \frac{d}{2N} \quad (4-18)$$

We take advantage of the integrability of the logarithmic singularity, exchange the integral and the summation sign with each other, and integrate term by term to obtain

$$A_{\ell\ell} = \frac{e^{-ik\Delta} - 1}{k^2 a} - \frac{\cot kc}{kN} + 2 \sum_{m=1}^{\infty} \frac{e^{-ik_x \Delta} - 1}{k_x^2 a} - \sum_{m=1}^{\infty} \frac{\cot k_x c}{k_x m\pi} \left[\sin \frac{m\pi}{2N} (4\ell - 1) - \sin \frac{m\pi}{2N} (4\ell - 3) + 2 \sin \frac{m\pi}{2N} \right] \quad (4-19)$$

Although we overcame the singularities by choosing the proper expansion function and testing function, the summations in $A_{\ell n}$ and $A_{\ell\ell}$ converge slowly. We shall find ways to speed the convergence of these summations in the next section.

4.3 Improvement of Convergence

In this section, the asymptotic terms in the summations of the matrix elements will be found first, and will then be added to, and subtracted from the matrix elements to speed the convergence. Finally, the formulations of these elements, which are used to perform the numerical work, are presented.

The summations in the matrix elements converge slowly. To improve the convergence, we first note that the following terms have asymptotic behaviors as m approaches infinity:

$$\frac{e^{-ik_x x}}{ak_x^2} \longrightarrow -a \frac{e^{-\frac{m\pi}{a} x}}{(m\pi)^2} \quad (4-20)$$

$$\frac{\cot k_x c}{k_x m\pi} \sin mx \longrightarrow -\frac{d}{m^2 \pi^2} \sin mx \quad (4-21)$$

Note that the summation

$$\sum_{m=1}^{\infty} \frac{\sin mx}{m^2} = f(x) \quad (4-22)$$

is called Clausen's integral and there exists an algorithm to speed its convergence (Abramowitz and Stegun, 1964). Invoking Euler's identity,

$$\begin{aligned} \sum_{m=1}^{\infty} \frac{e^{-mx}}{m^2} &= \sum_{m=1}^{\infty} \frac{e^{i(imx)}}{m^2} \\ &= \sum_{m=1}^{\infty} \left(\frac{\cos imx}{m^2} + i \frac{\sin imx}{m^2} \right) \\ &= \sum_{m=1}^{\infty} \left(\frac{\cos my}{m^2} + i \frac{\sin my}{m^2} \right) \\ &= \sum_{m=1}^{\infty} \frac{\cos my}{m^2} + if(y) \end{aligned} \quad (4-23)$$

where $y = ix$. The second summation on the right hand side of equation (4-23) is the same as (4-22). Abramowitz and Stegun (1964) give an analytic result for the first summation on the right hand side of (4-23) in which the argument is real. The result is also valid for complex arguments.

The asymptotic terms (4-20) and (4-21) are added to equations (4-17) and (4-19), and the results can be recognized as the special functions for which quick numerical algorithms exist. On the other hand, when the asymptotic terms are subtracted from the original terms, the resulting combinations of summations converge rapidly. After rearranging the terms, the final results are:

$$\begin{aligned}
A_{ln} &= \frac{e^{-ik\Delta(2\ell-2n+1)} - e^{-ik\Delta(2\ell-2n-1)}}{2k^2 a} \\
&+ \sum_{m=1}^{\infty} \left[\frac{1}{k_x^2 a} e^{-ik_x \Delta(2\ell-2n+1)} + \frac{a}{m^2 \pi^2} e^{-\frac{m\pi}{a} \Delta(2\ell-2n+1)} \right] \\
&- \sum_{m=1}^{\infty} \left[\frac{1}{k_x^2 a} e^{-ik_x \Delta(2\ell-2n-1)} + \frac{a}{m^2 \pi^2} e^{-\frac{m\pi}{a} \Delta(2\ell-2n-1)} \right] \\
&- \sum_{m=1}^{\infty} \frac{a}{m^2 \pi^2} \left[e^{-\frac{m\pi}{a} \Delta(2\ell-2n+1)} - e^{-\frac{m\pi}{a} \Delta(2\ell-2n-1)} \right] - \frac{\cot kc}{kN} \\
&- \sum_{m=1}^{\infty} \left[\frac{2 \cot k_x c}{k_x m \pi} + \frac{d}{m^2 \pi^2} \right] \left[\sin \frac{m\pi}{2N} (2\ell + 2n - 1) - \sin \frac{m\pi}{2N} (2\ell + 2n - 3) \right. \\
&\quad \left. - \sin \frac{m\pi}{2N} (2\ell - 2n - 1) + \sin \frac{m\pi}{2N} (2\ell - 2n + 1) \right] \\
&+ \sum_{m=1}^{\infty} \frac{d}{m^2 \pi^2} \left[\sin \frac{m\pi}{2N} (2\ell + 2n - 1) - \sin \frac{m\pi}{2N} (2\ell + 2n - 3) \right. \\
&\quad \left. - \sin \frac{m\pi}{2N} (2\ell - 2n - 1) + \sin \frac{m\pi}{2N} (2\ell - 2n + 1) \right] \tag{4-24}
\end{aligned}$$

and

$$\begin{aligned}
A_{ll} &= \frac{e^{-ik\Delta} - 1}{k^2 a} - \frac{\cot kc}{kN} + 2 \sum_{m=1}^{\infty} \left[\frac{e^{-ik_x \Delta} - 1}{k_x^2 a} + \frac{a}{m^2 \pi^2} \left(e^{-\frac{m\pi \Delta}{a}} - 1 \right) \right] \\
&- 2 \sum_{m=1}^{\infty} \frac{a}{m^2 \pi^2} e^{-\frac{m\pi \Delta}{a}} + \frac{a}{3} - \sum_{m=1}^{\infty} \left[\frac{\cot k_x c}{k_x m \pi} + \frac{d}{m^2 \pi^2} \right] \\
&\times \left[\sin \frac{m\pi}{2N} (4\ell - 1) - \sin \frac{m\pi}{2N} (4\ell - 3) + 2 \sin \frac{m\pi}{2N} \right] \\
&+ \sum_{m=1}^{\infty} \frac{d}{m^2 \pi^2} \left[\sin \frac{m\pi}{2N} (4\ell - 1) - \sin \frac{m\pi}{2N} (4\ell - 3) + 2 \sin \frac{m\pi}{2N} \right] \tag{4-25}
\end{aligned}$$

The efficiency of the addition and subtraction of (4-20) and (4-21) is demonstrated in Tables 4-1 and 4-2, where we show the results of the summations (4-20) and (4-21) summed directly for various x , the number of terms employed, the true value, and the relative error.

After evaluating all matrix elements $A_{\ell n}$, the matrix $[A_{\ell n}]$ is known. The source vector $[F_{\ell}]$ is known, too. Hence, the coefficients of the series α_n , where $n = 1, 2, \dots, N$, can be determined by finding the inverse matrix $[A_{\ell n}]^{-1}$. Finally, we solve for the approximation to the aperture field $E_A(z')$ in (4-11).

4.4 Reflection Coefficient by MOM

In this section, we shall use the results of MOM to derive the reflection coefficient. The procedure is similar to the low frequency case. We are still concerned only with the reflected wave of the TEM mode. In this case, the magnetic field for $-p < z < 0$ can be written as

$$\begin{aligned} H_{y1}(x, z) &= -i\omega\epsilon \frac{e^{-ik(z+p)}}{2ik} - i\omega\epsilon \int_0^d \frac{e^{ik(z-z')}}{2ika} \sum_{n=1}^N \alpha_n P_n(z') dz' \\ &= -i\omega\epsilon \frac{e^{-ik(z+p)}}{2ik} - i\omega\epsilon \sum_{n=1}^N \frac{\alpha_n}{2k^2 a} \left[(1 - e^{ik\frac{d}{N}}) e^{ik(z - \frac{nd}{N})} \right] \quad (4-26) \end{aligned}$$

From the TM mode equations,

$$\begin{aligned} E_x &= -\frac{1}{i\omega\epsilon} \frac{\partial H_y}{\partial z} \\ &= -\frac{e^{-ik(z+p)}}{2} + \sum_{n=1}^N \frac{\alpha_n i}{2ka} \left[(1 - e^{ik\frac{d}{N}}) e^{ik(z - \frac{nd}{N})} \right] \quad (4-27) \end{aligned}$$

Table 4-1 Number of terms of convergence for $\sum_{m=1}^{\infty} \frac{\sin mx}{m^2}$

x	True Value	Summation	Terms	Relative Error
6.000	$-6.4078266 \times 10^{-1}$	$-6.4079596 \times 10^{-1}$	500	2.0755869×10^{-5}
6.000	$-6.4078266 \times 10^{-1}$	$-6.4077969 \times 10^{-1}$	1000	4.6349569×10^{-6}
4.000	$-5.6814395 \times 10^{-1}$	$-5.6814242 \times 10^{-1}$	500	2.6929795×10^{-6}
4.000	$-5.6814395 \times 10^{-1}$	$-5.6814329 \times 10^{-1}$	1000	1.1616774×10^{-6}
3.000	9.8026218×10^{-2}	9.8026260×10^{-2}	510	4.2845680×10^{-7}
3.000	9.8026218×10^{-2}	9.8026020×10^{-2}	800	2.0198678×10^{-6}
1.000	1.0139591×10^0	1.01391527×10^0	150	4.3295632×10^{-5}
1.000	1.0139591×10^0	1.01396144×10^0	500	2.2683361×10^{-6}
0.100	3.3027240×10^{-1}	3.3027109×10^{-1}	2000	4.2389252×10^{-6}
0.100	3.3027240×10^{-1}	3.3027237×10^{-1}	3000	9.0834111×10^{-8}
0.010	5.6051716×10^{-2}	5.6039555×10^{-2}	2000	2.1696035×10^{-4}
0.010	5.6051716×10^{-2}	5.6050681×10^{-2}	3000	1.8465090×10^{-5}
0.010	5.6051716×10^{-2}	5.6055661×10^{-2}	4000	7.0381431×10^{-5}
0.010	5.6051716×10^{-2}	5.6047902×10^{-2}	5000	6.8044304×10^{-5}
0.001	7.907755×10^{-3}	7.4041089×10^{-3}	1000	6.3690150×10^{-2}
0.001	7.907755×10^{-3}	7.9094912×10^{-3}	5000	2.1955663×10^{-4}
0.001	7.907755×10^{-3}	7.9166983×10^{-3}	10000	1.1309531×10^{-3}
0.001	7.907755×10^{-3}	7.9065290×10^{-3}	20000	1.5503768×10^{-4}
0.001	7.907755×10^{-3}	7.9073744×10^{-3}	50000	4.8129969×10^{-5}
0.001	7.907755×10^{-3}	7.9076701×10^{-3}	100000	1.0736296×10^{-5}

Table 4-2 Number of terms of convergence for $\sum_{m=1}^{\infty} \frac{e^{-mz}}{m^2}$

z	True Value	Summation	Terms	Relative Error
0.100	1.3121894	1.2990876	10	9.9846867×10^{-3}
0.100	1.3121894	1.3121890	80	3.0483404×10^{-7}
0.010	1.5888574	1.5209690	10	4.2727812×10^{-2}
0.010	1.5888574	1.5873907	100	9.2311620×10^{-4}
0.010	1.5888574	1.5888221	300	2.2154285×10^{-5}
0.010	1.5888574	1.5888554	500	1.2587662×10^{-6}
0.001	1.6370261	1.6298457	100	4.3862465×10^{-3}
0.001	1.6370261	1.6368777	1000	9.0652189×10^{-5}
0.001	1.6370261	1.6370073	2000	1.1484240×10^{-5}
0.001	1.6370261	1.6370225	3000	2.1991097×10^{-6}

The voltage across the waveguide can be determined by integrating equation (4-27), viz:

$$\begin{aligned}
 V &= \int_0^a E_x dx \\
 &= -a \frac{e^{-ik(z+p)}}{2} + \sum_{n=1}^N \frac{\alpha_n i}{2k} \left[(1 - e^{ik\frac{d}{N}}) e^{ik(z - \frac{nd}{N})} \right] \quad (4-28)
 \end{aligned}$$

Comparing the reflected voltage with the incident voltage in the voltage expression, we obtain the following reflection coefficient:

$$\Gamma(\omega) = -\frac{\sum_{n=1}^N \alpha_n i \left(1 - e^{ik\frac{d}{N}} \right) e^{ik(z - \frac{nd}{N})}}{kae^{-ik(z+p)}} \quad (4-29)$$

Note that, although we have discarded all higher order modes at the observation point where we calculate Γ , the higher order mode effects in the aperture are contained in the sequence $\{\alpha_n\}$.

4.5 Numerical Results

In this section, we will present the numerical results from the formulations we derived previously. Before presenting the results, we replace k in (2-48), (4-24), (4-25) and (4-29) by the relation (3-19), and set $z = 0$ and $p = 0$ in (2-48) and (4-29).

Fig 4-2 through Fig 4-6 are plots of the product of the amplitude of the aperture electrical field distribution $|E_A|$ and the width of the aperture d versus different N (the number of intervals in the aperture) for the parameters $a = 2$, $d/a = 0.044$, $c/a = 1.33$, and $k = 0.706$. The larger N becomes, the closer to

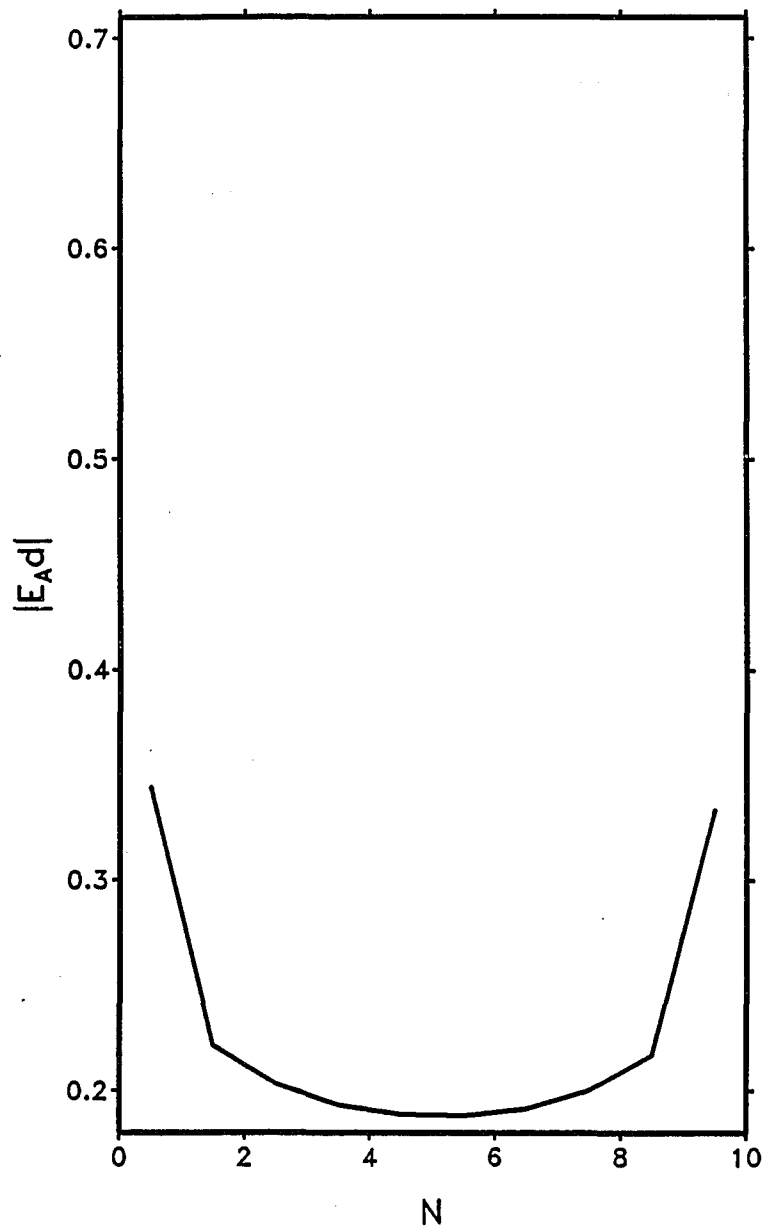


Figure 4-2 The product of the amplitude of the aperture field distribution E_A and the width of the aperture d , with $a = 2$, $d/a = 0.044$, $c/a = 1.33$, $k = 0.706$, and $N = 10$.

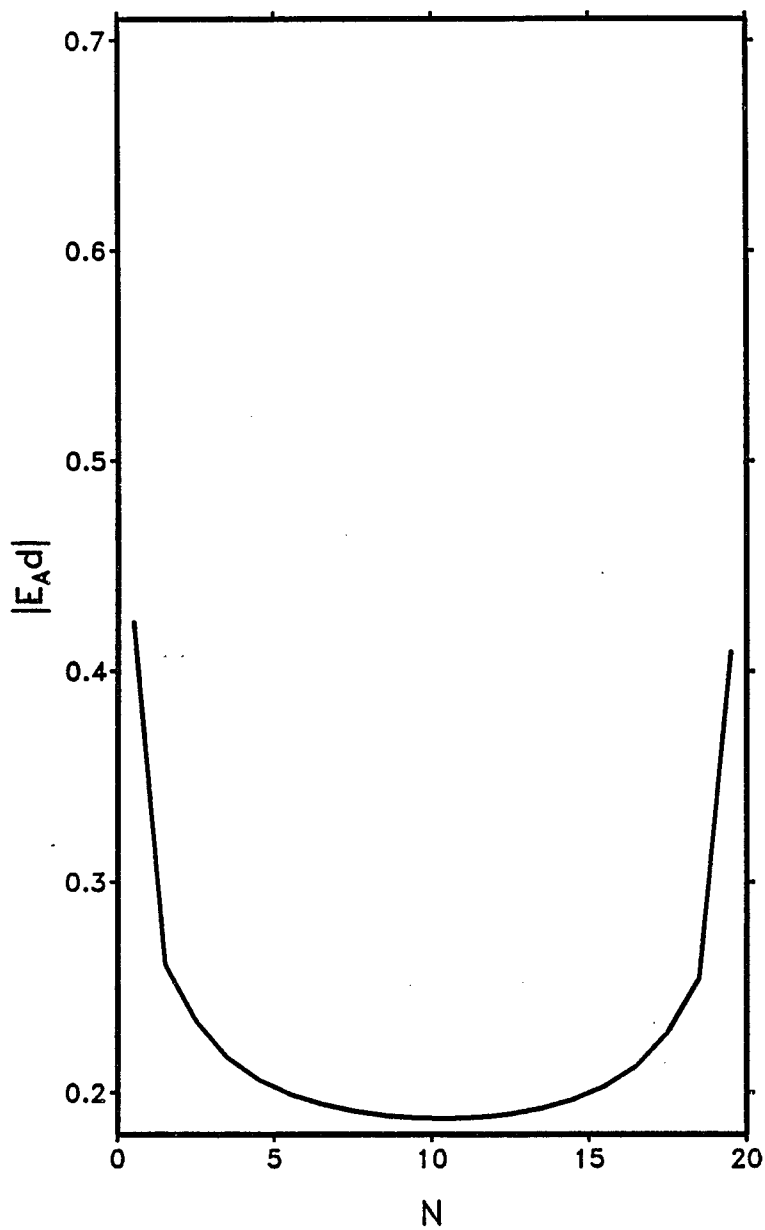


Figure 4-3 The product of the amplitude of the aperture field distribution E_A and the width of the aperture d , with $a = 2$, $d/a = 0.044$, $c/a = 1.33$, $k = 0.706$, and $N = 20$.

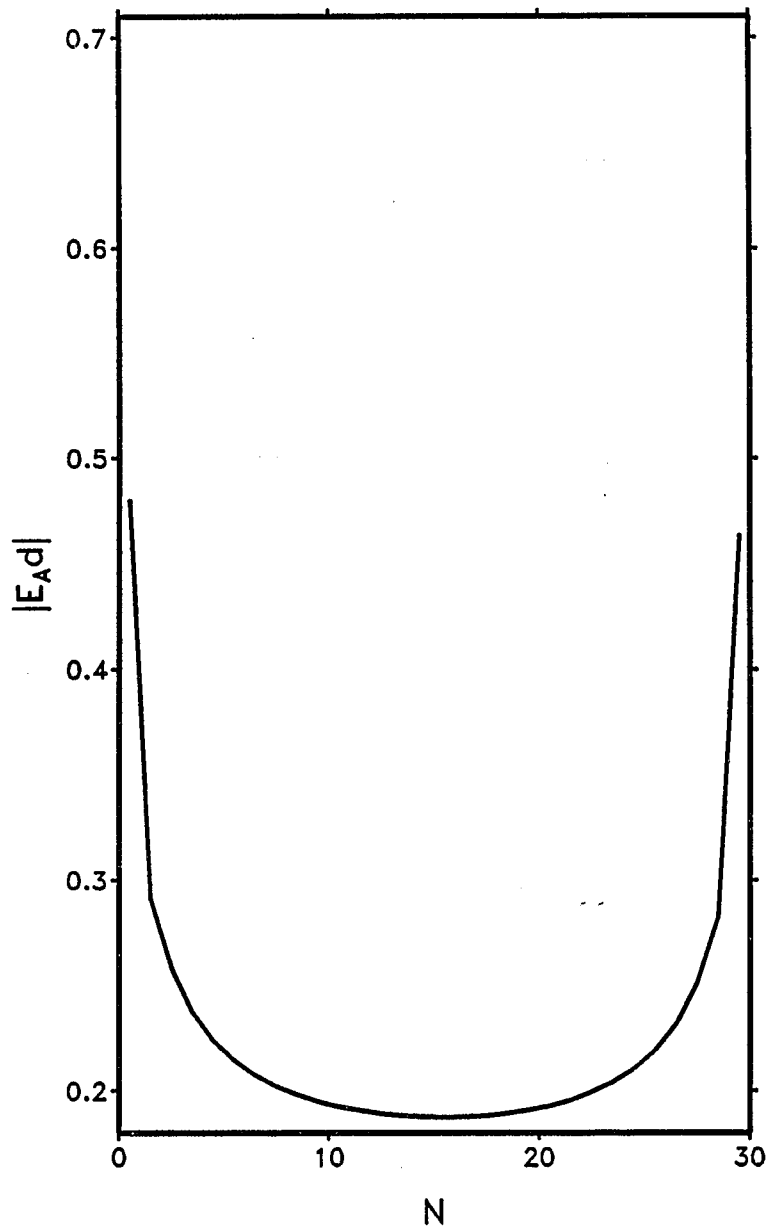


Figure 4-4 The product of the amplitude of the aperture field distribution E_A and the width of the aperture d , with $a = 2$, $d/a = 0.044$, $c/a = 1.33$, $k = 0.706$, and $N = 30$.

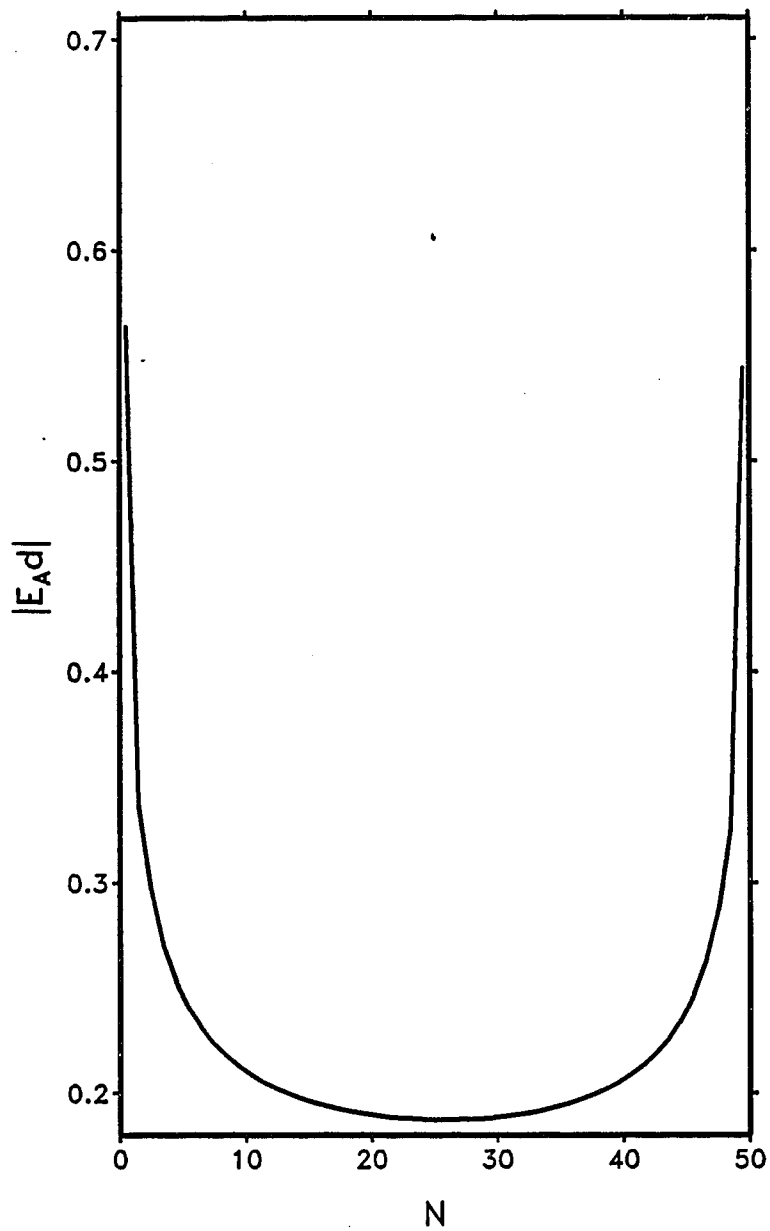


Figure 4-5 The product of the amplitude of the aperture field distribution E_A and the width of the aperture d , with $a = 2$, $d/a = 0.044$, $c/a = 1.33$, $k = 0.706$, and $N = 50$.

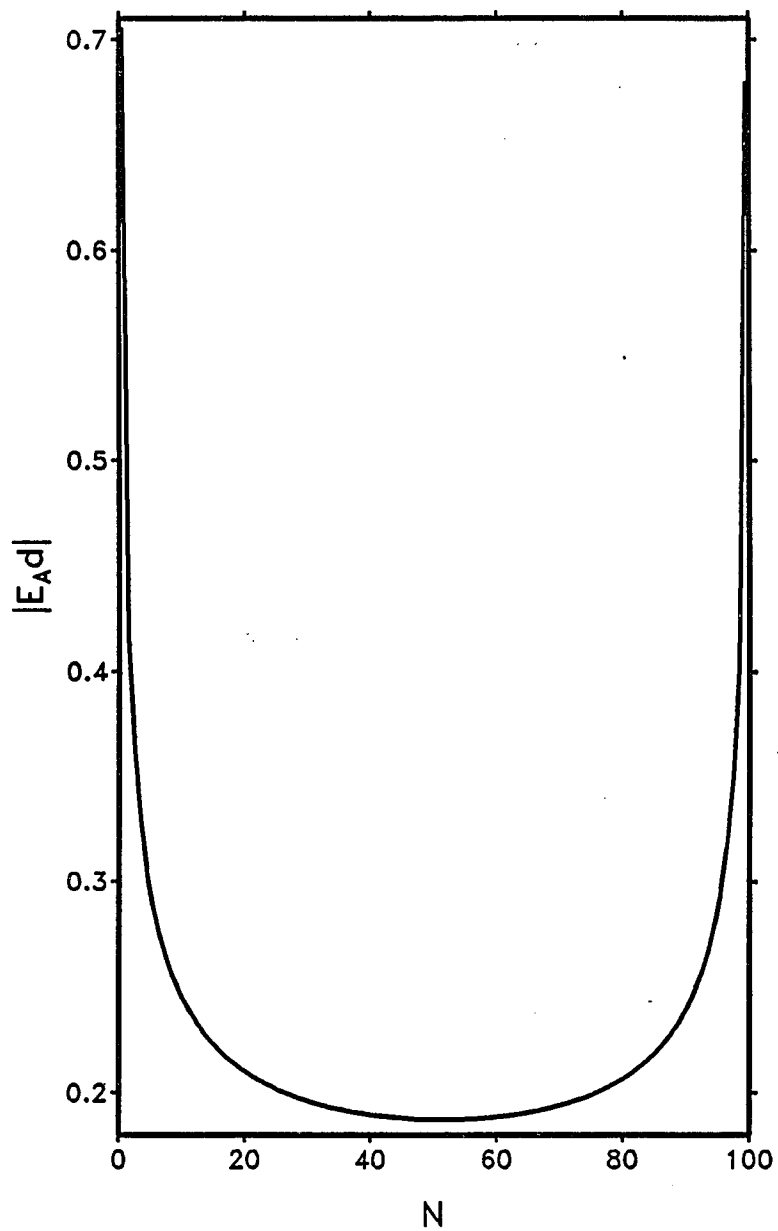


Figure 4-6 The product of the amplitude of the aperture field distribution E_A and the width of the aperture d , with $a = 2$, $d/a = 0.044$, $c/a = 1.33$, $k = 0.706$, and $N = 100$.

the edges the observation points move. It can be seen that the minimum values of $|E_{Ad}|$ are similar; however, the maximum values of each curve are different, implying that the field distributions near the edges become large as N increases. This behaviour is due to the edge singularities at $z = 0$ and $z = d$ which we predicted in section 4-1.

The amplitude of the reflection coefficient versus N is plotted in Fig 4-7. It is clear that when N is greater than or equal to 20, $|\Gamma|$ is virtually independent of N . Henceforth, we frequently use $N = 30$ for further computations.

The amplitude of the reflection coefficient versus the ratio c/λ is presented in Fig 4-8 for the following geometric dimensions: $a = 2$, $d/a = 1.333$, $k = 0.706$, and $N = 30$ (plotted here for $0.0 < c/\lambda < 1.0$). It is observed that the reflection coefficient $|\Gamma|$ has resonant characteristics and varies periodically vs. c/λ . When $c/\lambda \approx 0.25, 0.75$, $|\Gamma| \rightarrow 1$, and when $c/\lambda \approx 0.50, 1.0$, $|\Gamma| \rightarrow 0$. Invoking transmission line theory, for the former case, the input impedance of the branch line at its input reference plane is equivalent to an open circuit since the wave is unable to propagate and is completely reflected ($|\Gamma| \rightarrow 1$). The input impedance of the branch line at its reference plane for the latter case, however, is equivalent to a short circuit since $|\Gamma| \rightarrow 0$, and the branch line appears absent. According to transmission line theory, the maximum values of the reflection coefficient must take place at $0.25\lambda, 0.75\lambda$, etc., and the minimum values of the reflection coefficient must take place at $0.5\lambda, 1.0\lambda$, etc. for an ideal transmission line. However, the peak values of the reflection coefficient shift slightly to the left in Fig 4-8, meaning that

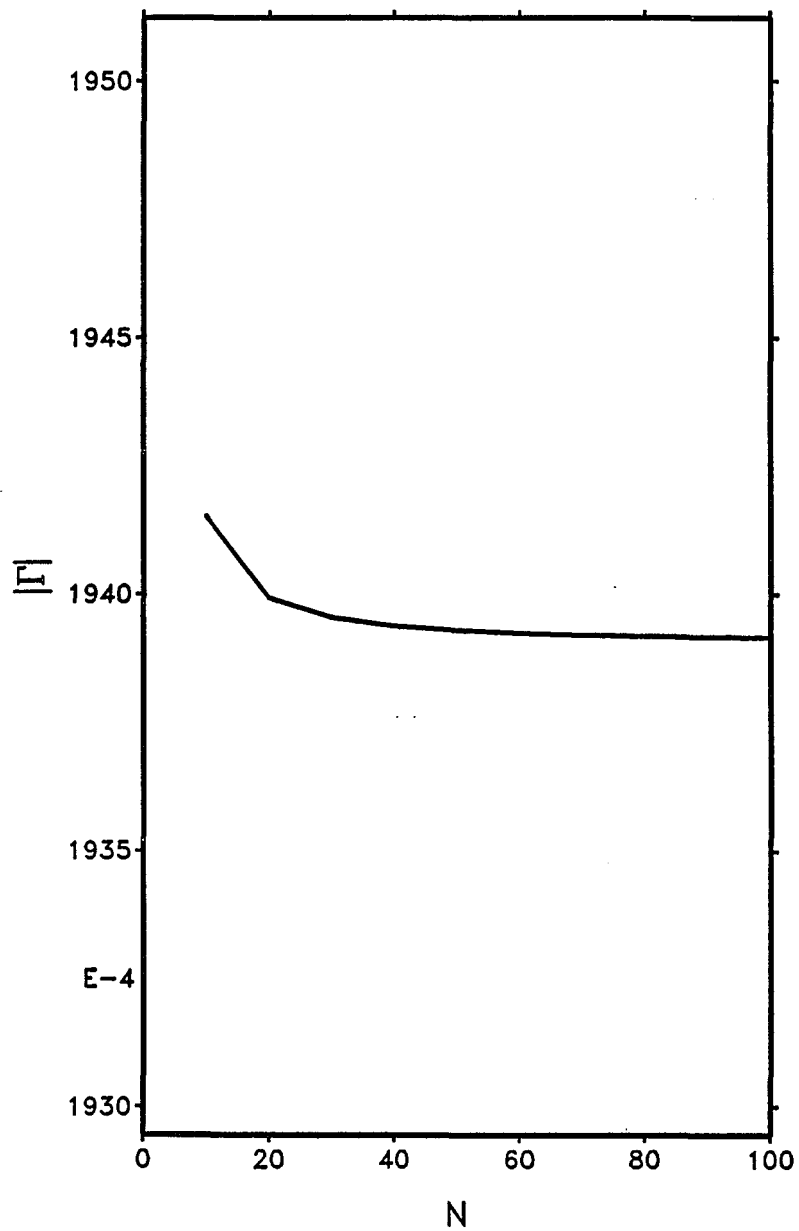


Figure 4-7 The amplitude of the reflection coefficient by MOM as a function of N , where $a = 2$, $d/a = 0.444$, $c/a = 1.554$, and $k = 0.706$.

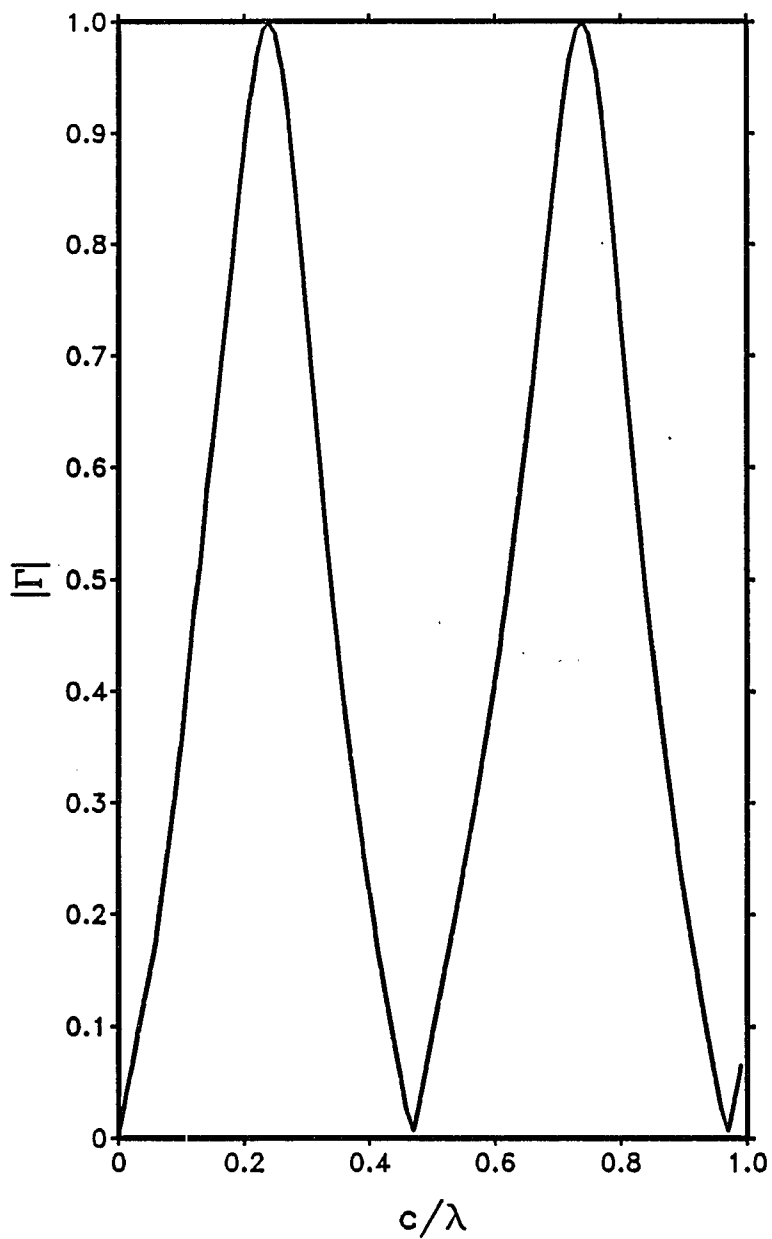


Figure 4-8 The amplitude of the reflection coefficient by MOM as a function of c/λ , where $a = 2$, $d/a = 1.33$, and $k = 0.706$.

the resonant frequency f_r becomes lower. From circuit theory, the definition of the resonant frequency of a LC circuit is (Huelsman, 1984)

$$f_r = \frac{1}{2\pi\sqrt{LC}} \quad (4 - 30)$$

Therefore, increasing both L or C will cause f_r to decrease. The corners of the aperture give rise to high charge concentrations compared to other regions in the waveguide and branch line. This effect is equivalent to an extra discontinuous structure capacitor at the aperture; therefore, the shift of the resonance curve is caused by this structure capacitor.

Fig 4-9 shows the amplitude of the reflection coefficient as a function of the ratio d/λ . As we expect, the reflection coefficient approaches zero as the ratio d/λ becomes smaller and smaller. This phenomenon is in accord with the real physical situation: as the width of the aperture becomes smaller and smaller, the effects of the branch line vanish.

Fig 4-10 and Fig 4-11 are plots of the amplitude of the reflection coefficient versus the normalized angular frequency ω/ω_c , where ω is the operating angular frequency and ω_c is the cutoff angular frequency of the first higher order mode in the main waveguide. Both plots have the parameters $a = 1.5$ and $c/a = 4.666$, but the d/a parameters are different, being equal to 1.166 for Fig 4-10 and 0.666 for Fig 4-11. In Fig 4-10, there are visible irregularities which occur when $\omega/\omega_c \geq 0.85$, which is the first higher mode cutoff frequency in the branch line. This phenomenon is caused by the existence of the higher mode wave in the branch line when the operating frequency is higher than the cutoff frequency. It is the existence of the

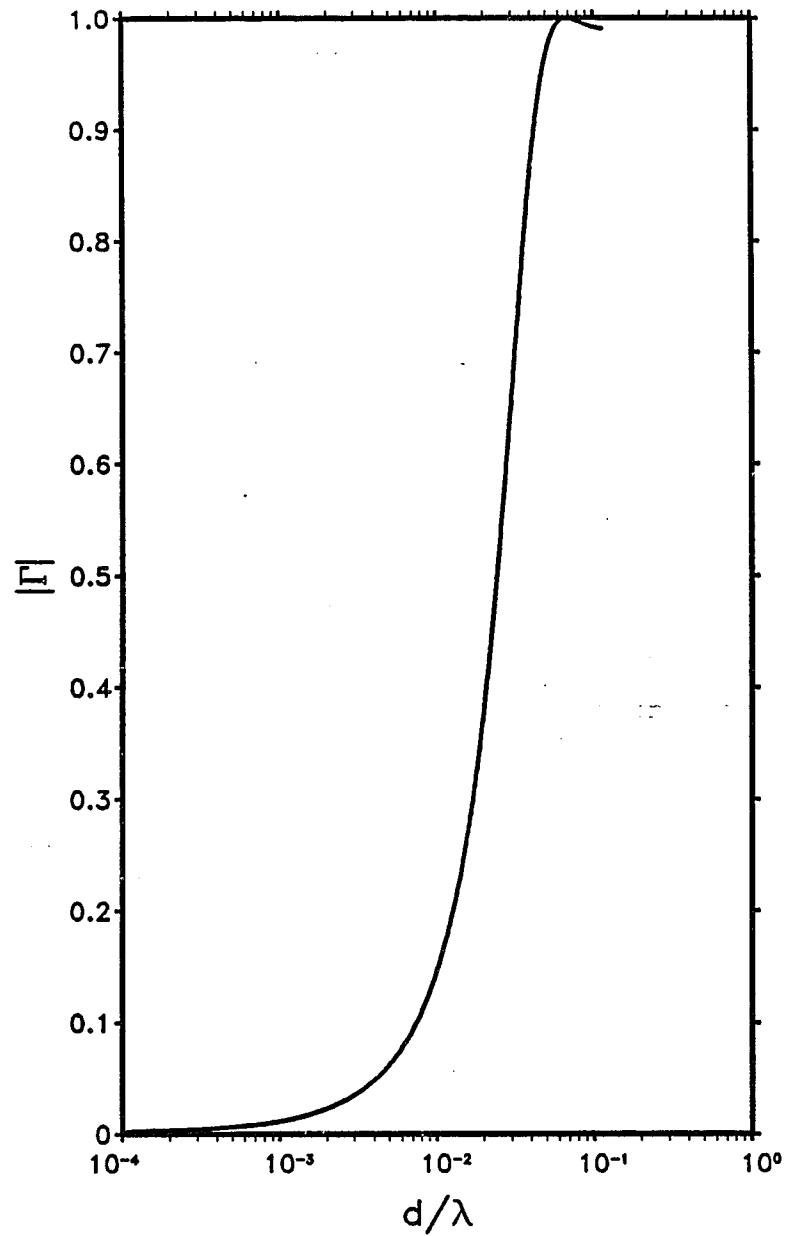


Figure 4-9 The amplitude of the reflection coefficient by MOM as a function of d/λ , where $a = 2$, $c/a = 0.955$, and $k = 0.706$.

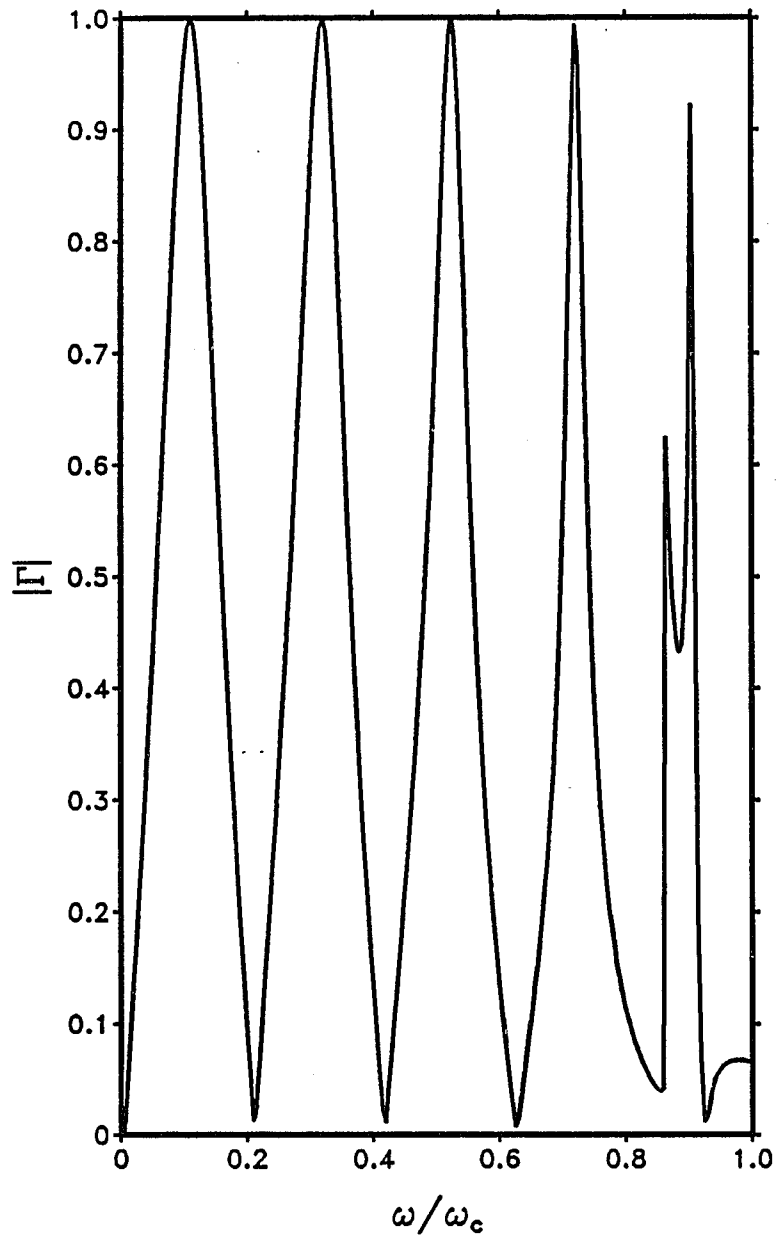


Figure 4-10 The amplitude of the reflection coefficient by MOM as a function of ω/ω_c , where $a = 1.5$, $d/a = 1.166$, and $c/a = 4.666$. ($\omega_c = 6.28 \times 10^8$ radians/second)

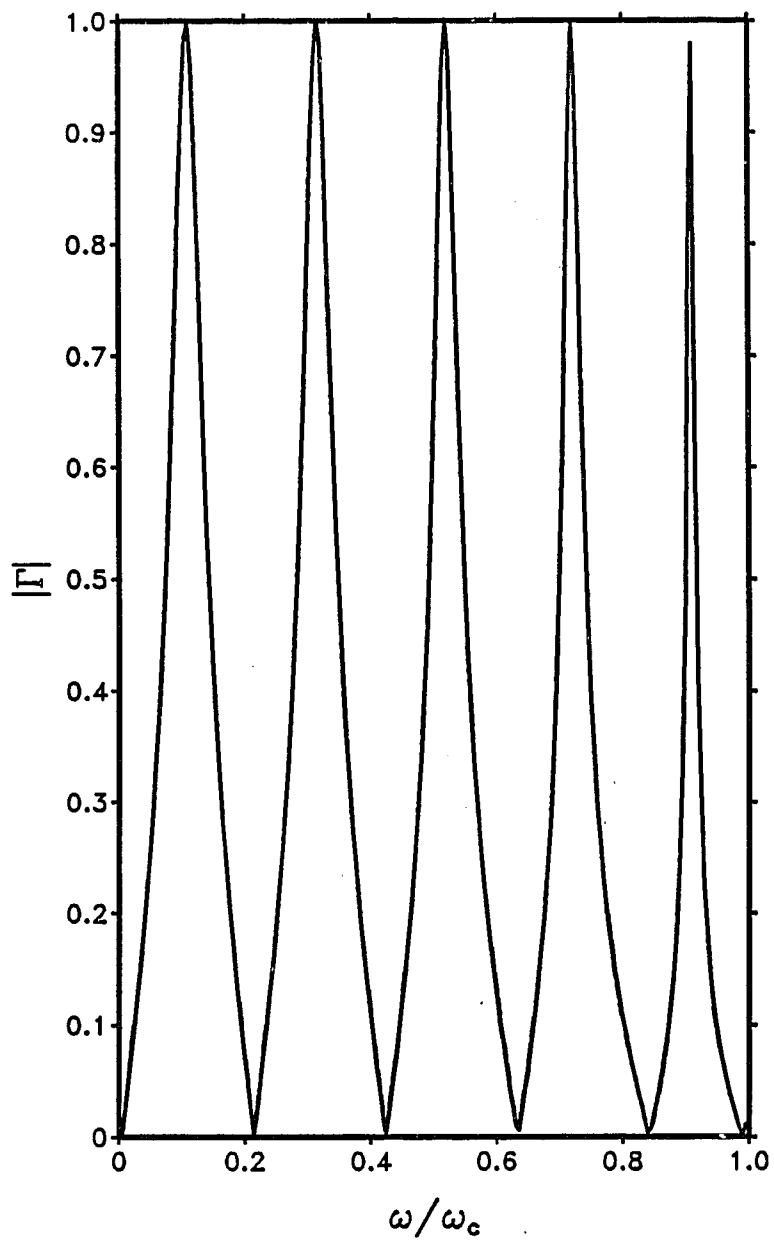


Figure 4-11 The amplitude of the reflection coefficient by MOM as a function of ω/ω_c , where $a = 1.5$, $d/a = 0.666$, and $c/a = 4.666$. ($\omega_c = 6.28 \times 10^8$ radians/second)

higher mode wave that affects the local shape of the reflection coefficient waveform. On the contrary, Fig 4-11 does not reveal this feature since the operating frequency is lower than the first cutoff frequency in the branch line and the higher mode wave does not appear. Recall that as $c/\lambda = 0.25, 0.75, \dots$, Γ takes on a maximum value and as $c/\lambda = 0.5, 1.0, \dots$, Γ takes on a minimum value. For the curve shown in Fig 4-11, the values of $\omega/\omega_c \approx 0.107, 0.321, 0.535, 0.750, 0.964$ correspond to $c/\lambda = 0.25, 0.75, 1.25, 1.75, 2.25$, respectively, and the values of $\omega/\omega_c \approx 0.214, 0.428, 0.644, 0.857$ correspond to $c/\lambda = 0.50, 1.0, 1.5, 2.0$, respectively. It can be seen that the results shown in Fig 4-11 agree with the calculated results at low frequencies, but at higher frequencies the peak values and node points of the reflection coefficient tend to shift to values below those of the calculated results (by approximately 2 ~ 3 %) despite the absence of the higher mode wave. This is due to the effects of the shunt capacitor which, according to circuit theory, becomes more prominent at higher frequencies.

Excluding the shift caused by the shunt capacitor, the superposition of the TEM mode and the higher mode fields make the situation much more complicated at high frequencies. Fig 4-12 presents the amplitude of the reflection coefficient versus the normalized frequency ω/ω_c with the parameters $a = 1.5$, $d/a = 1.5$, and $c/a = 4.666$. The shunt capacitor causes the peak values and node points to shift by approximately 2 ~ 3 % when $\omega/\omega_c > 0.4$. As ω/ω_c exceeds 0.666, the first higher mode appears in the branch line; therefore, the resonance characteristics of the curve can be considered a combination of the TEM mode and the higher mode. This can also be interpreted from basic transmission line theory. For example, resonances occur at $\omega/\omega_c = 0.67$ and 0.74 which correspond to the ratio $c/\lambda_g = 0.25$

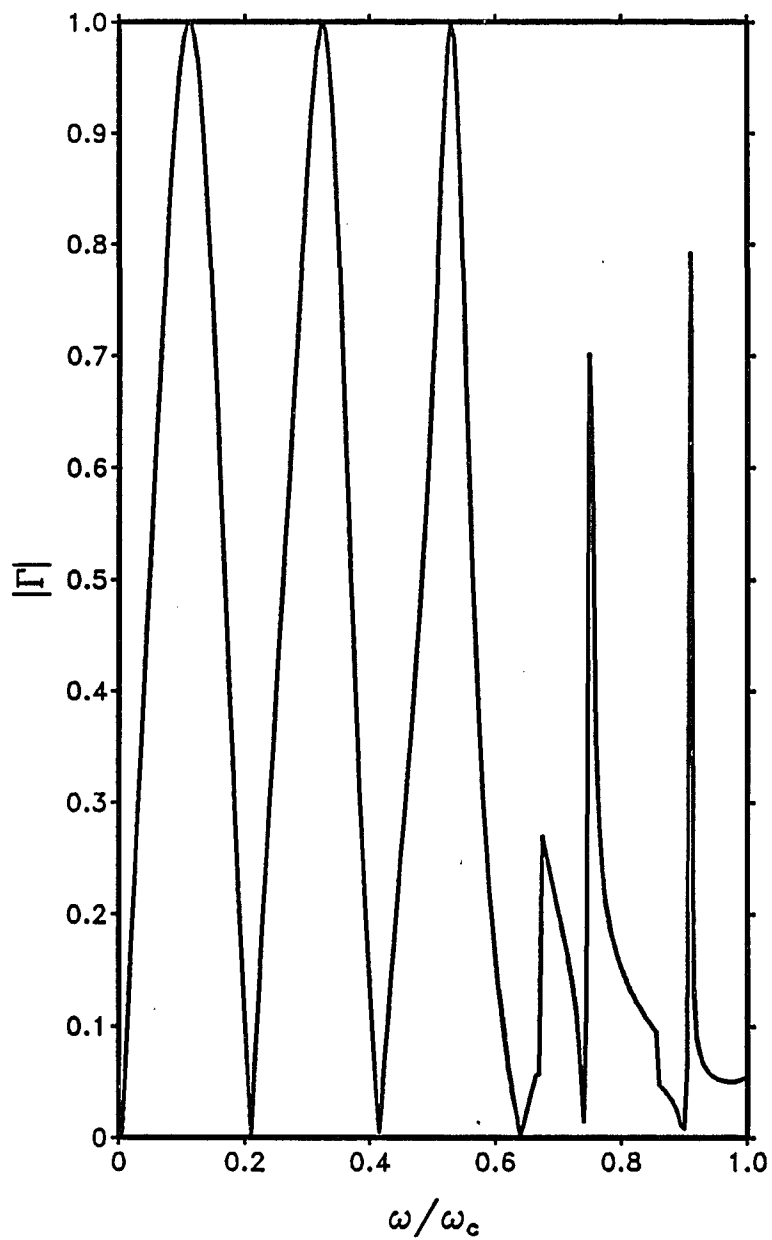


Figure 4-12 The amplitude of the reflection coefficient by MOM as a function of ω/ω_c , where $a = 1.5$, $d/a = 1.5$, and $c/a = 4.666$. ($\omega_c = 6.28 \times 10^8$ radians/second)

and 0.75, respectively, where λ_g is the guided wavelength in the branch line (to be distinguished from λ) (Liao, 1985),

$$\begin{aligned}\lambda_g &= \frac{\lambda}{\sqrt{1 - \left(\frac{\lambda}{\lambda_c}\right)^2}} \\ &= \frac{\lambda}{\sqrt{1 - \left(\frac{\lambda}{2d}\right)^2}}\end{aligned}\quad (4-31)$$

When $\omega/\omega_c = 0.7$, we would expect $|\Gamma|$ to have a value of zero since $c/\lambda_g \approx 0.50$ due to existence of the first higher order wave. $|\Gamma|$ however, is nonzero as can be seen from Fig 4-12. The finite value of $|\Gamma|$ is due to the presence of the TEM wave for which $c/\lambda \neq 0.50$.

We combine the amplitude of the reflection coefficient from MOM and from the low frequency approximation in Fig 4-13. In chapter 3 we showed that the TEM mode is the dominant term in the formulation of the low frequency approximation as long as $ka \cdot kc \ll 3$ (equation (3-13)). When $\omega/\omega_c = 0.09$, the calculated value of $ka \cdot kc$ is about 0.5. This result can be seen in Fig 4-13. Good agreement exists between the two curves when $\omega/\omega_c < 0.09$ which confirms that the low frequency approximation is valid under the restriction in equation (3-13), as we expected.

In this section, we have shown the numerical results computed by a VAX 11/750 computer. First of all, we presented the products of the amplitude distribution of the aperture field with the width of the aperture d . These results verify the theoretical prediction: there exist singularities at the edges. We have also proven that the amplitude distribution for a narrow aperture is in agreement with a physical model. Secondly, the graph of $|\Gamma|$ versus N has demonstrated how quickly

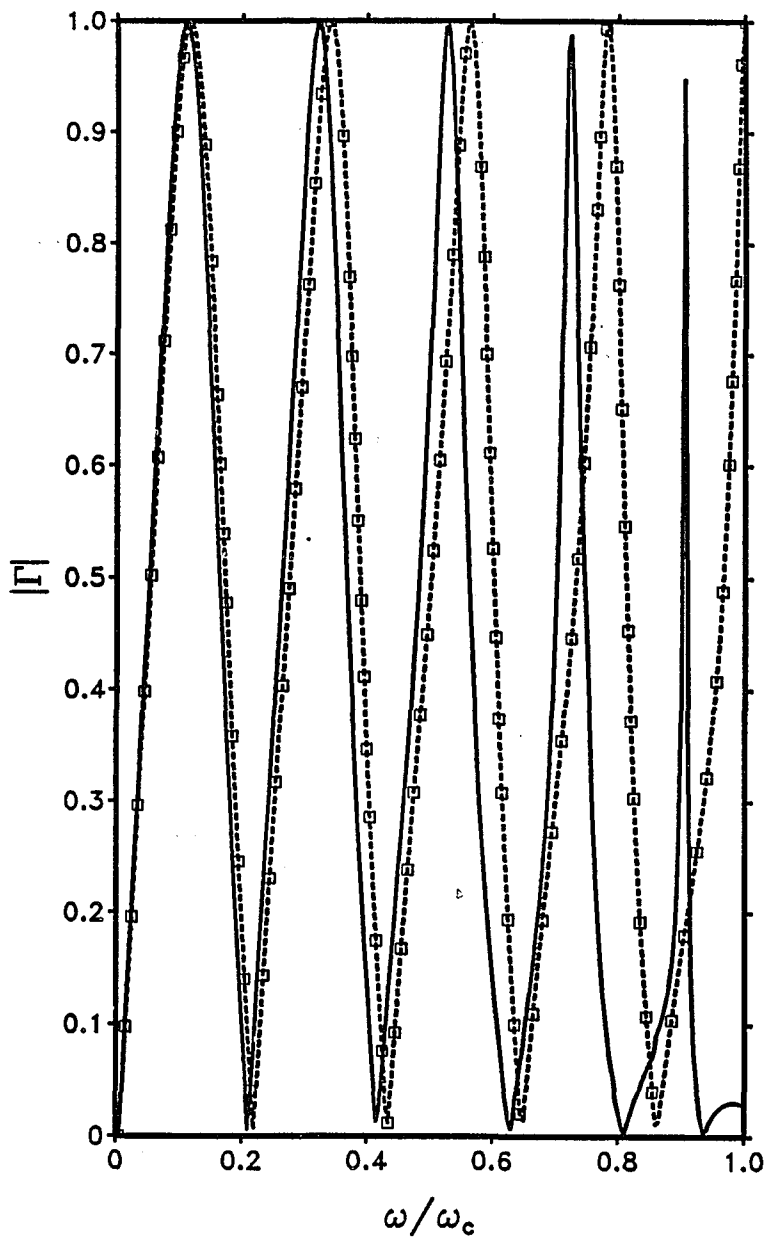


Figure 4-13 The solid line denotes $|\Gamma|$ by MOM as a function of ω/ω_c , and the dashed line with \square denotes $|\Gamma|$ using the low frequency approximation as a function of ω/ω_c , where $a = 1.5$, $d/a = 1.333$, and $c/a = 4.666$. ($\omega_c = 6.28 \times 10^8$ radians/second)

MOM converges. We then plotted the amplitude of the reflection coefficients versus c/λ , d/λ , and ω/ω_c . They are in good agreement with the conclusions from transmission line theory. Finally, a comparison was made of the reflection coefficients for the case where MOM was used and for the case where the low frequency approximation was used.

CHAPTER 5

TIME DOMAIN RESULTS

Having computed the reflection coefficient in the frequency domain by MOM in chapter 4, we can now determine the time response of the exciting signals in the waveguide by the Fourier transform method. It will be seen that there is a discontinuity in the slope of the transient response. This discontinuity is caused by the reflection of the wave from the bottom of the branch line when the double exponential pulse function is applied as an input.

In this chapter, we begin with a brief introduction of the basic principle of the Fourier transform method. We next discuss the input pulse – the double exponential pulse. Finally, we will display the numerical results.

5.1 Fundamentals of Fourier Transform Method

One of the most frequently used method for dealing with transient phenomena in time-invariant media is the Fourier integral transform technique. Here, the time variable in the field equations appears solely through the derivative operator $\partial/\partial t$. When the field equations are represented in terms of the exponential eigenfunctions $\exp(i\omega t)$, as in the Fourier transform, then the temporal dependence is removed. The resulting “time-harmonic” field is of interest in its own right, and from its solution the transient field is recovered by application of the inverse transform.

We treat our structure as a linear system. Since we are interested in the reflection coefficient in the main waveguide, the transfer function of this system is the expression of the reflection coefficient we obtained in the last chapter.

$$\Gamma(\omega) = -\frac{\sum_{n=1}^N \alpha_n i \left(1 - e^{ik\frac{d}{N}}\right) e^{ik\left(z - \frac{nd}{N}\right)}}{kae^{-ik(z+p)}} \quad (5-1)$$

where $k = 2\pi/\lambda = \omega/v_c$, and v_c is the speed of light in free space.

Physically, the transfer function is the response of the system for a δ -function input. According to linear system theory, if the transfer function of a system is known, the responses of the system for various exciting sources can be obtained theoretically by convolution. For most numerical cases, however, it is easier to employ a Fourier transform algorithm than to perform the convolution. Using the convolution property of the Fourier transform, if

$$f(t) \xleftrightarrow{\mathcal{F}} F(\omega) = \int_{-\infty}^{\infty} f(t) e^{-i\omega t} dt \quad (5-2)$$

$$h(t) \xleftrightarrow{\mathcal{F}} H(\omega) = \int_{-\infty}^{\infty} h(t) e^{-i\omega t} dt \quad (5-3)$$

where $f(t)$ is the exciting signal and $h(t)$ is the δ -function response, then

$$f(t) * h(t) \xleftrightarrow{\mathcal{F}} F(\omega)H(\omega) \quad (5-4)$$

Therefore,

$$f(t) * h(t) = \mathcal{F}^{-1}\{F(\omega)H(\omega)\} \quad (5-5)$$

In our problem, $H(\omega)$ is $\Gamma(\omega)$ which is known; therefore, we are able to obtain the time response of the reflection coefficient when the exciting signal is properly selected. We will discuss the input signal in the next section.

To sum up, the procedure used to solve the transient problem by the Fourier integral transform method is:

(1) Solve the corresponding problem in the frequency domain in order to obtain the system response as a function of frequency.

(2) Find the spectral function of the exciting signal using the Fourier transform.

(3) Perform the inverse Fourier transform of the product of the system response in the frequency domain with the spectral function of the exciting signal so that the system response in time domain is solved.

5.2 Exciting Signal

We choose the normalized double exponential pulse function to be the input pulse, i.e.,

$$f(t) = A_0(e^{-\alpha t} - e^{-\beta t})u(t) \quad (5-6)$$

where $u(t)$ is the unit step function and A_0 is a normalization factor so that the maximum of $f(t)$ is unity. Since $f(t)$ has only one local maximum at $t = t_0$, we can find A_0 and t_0 by applying simple calculus rules.

For $t > 0$, we set the derivative of $f(t)$ equal to zero at $t = t_0$, viz:

$$\left. \frac{df}{dt} \right|_{t=t_0} = A_0(-\alpha e^{-\alpha t_0} + \beta e^{-\beta t_0}) = 0 \quad (5-7)$$

If $A_0 \neq 0$ then

$$\frac{\beta}{\alpha} e^{-\beta t_0} = e^{-\alpha t_0} \quad (5-8)$$

or

$$\ln \frac{\beta}{\alpha} - \beta t_0 = -\alpha t_0 \quad (5-9)$$

which can be solved for t_0 to give

$$t_0 = \frac{1}{\beta - \alpha} \ln \frac{\beta}{\alpha} \quad (5-10)$$

We now find A_0 by setting the maximum value of $f(t)$ equal to 1, i.e.,

$$f(t_0) = A_0(e^{-\alpha t_0} - e^{-\beta t_0}) = 1 \quad (5-11)$$

and solve for A_0 to obtain

$$A_0 = \frac{1}{e^{-\alpha t_0} - e^{-\beta t_0}} \quad (5-12)$$

The advantage in choosing the double exponential pulse function as the input signal is that this function can practically simulate either the step function or the δ -function by properly adjusting both α and β .

We perform the Fourier transform of equation (5-6), yielding the spectral function

$$F(\omega) = \mathcal{F}[f(t)] = \int_{-\infty}^{\infty} f(t)e^{-i\omega t} dt = A_0 \left(\frac{1}{\alpha + i\omega} - \frac{1}{\beta + i\omega} \right) \quad (5-13)$$

Fig 5-1 and Fig 5-2 are plots of the normalized double exponential pulse function and its spectral function, respectively $\alpha = 1.0 \times 10^7$ and $\beta = 1.0 \times 10^8$.

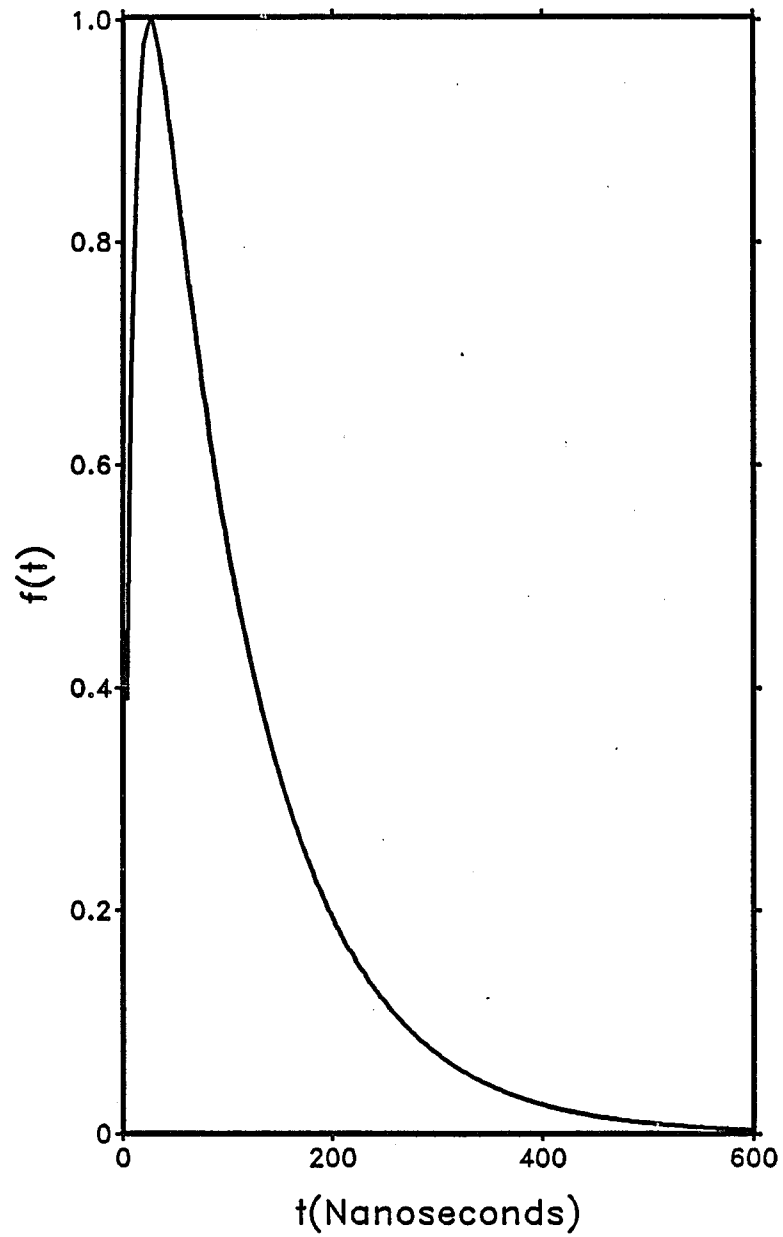


Figure 5-1 The double exponential pulse function with the parameters $\alpha = 1.0 \times 10^7$ and $\beta = 1.0 \times 10^8$.

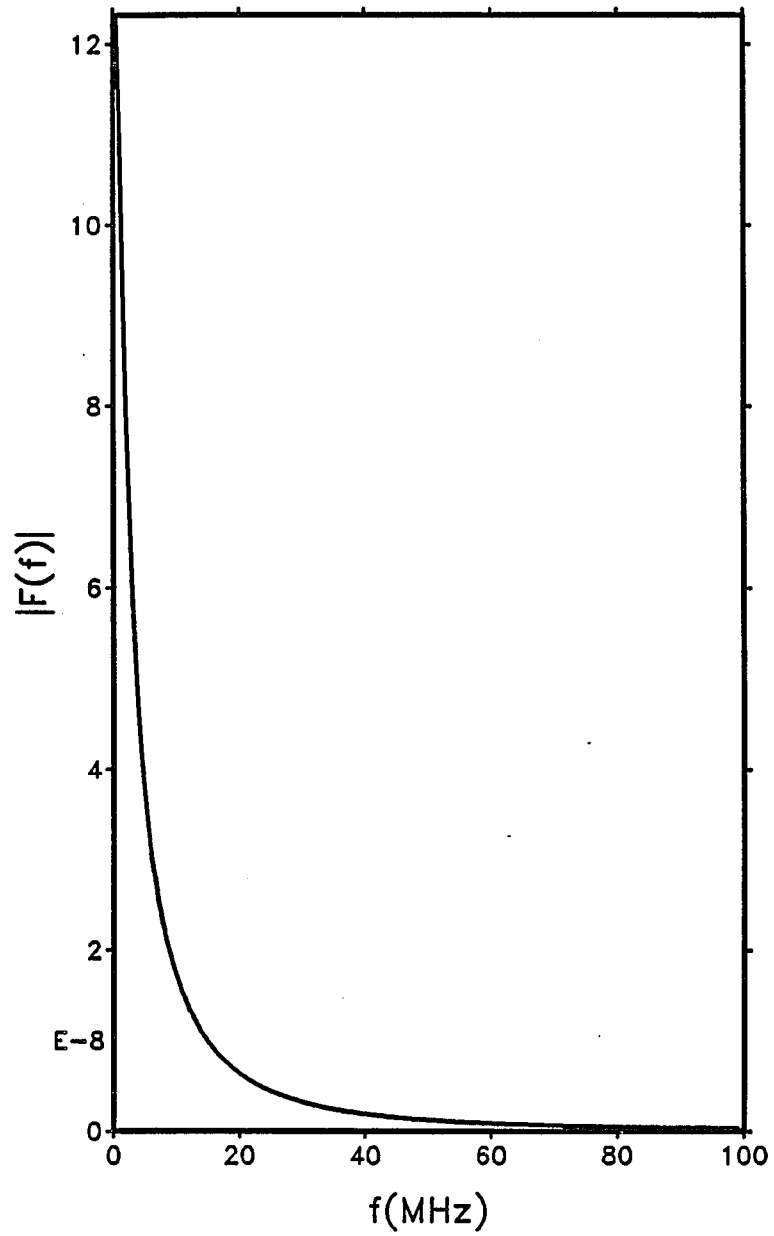


Figure 5-2 The spectral function of the double exponential function with the parameters $\alpha = 1.0 \times 10^7$ and $\beta = 1.0 \times 10^8$.

5.3 Analysis of Transient Responses

Recall that we set $z = 0$ and $p = 0$ when we obtained the numerical results for the frequency domain solutions in the last chapter. In this case, the transient response of the system $g(t)$ for a given input pulse $f(t)$ is the inverse Fourier transform,

$$\begin{aligned}
 g(t) &= \mathcal{F}^{-1}[F(\omega) + \Gamma(\omega) \cdot F(\omega)] \\
 &= f(t) + \frac{1}{2\pi} \int_{-\infty}^{\infty} \Gamma(\omega) \cdot F(\omega) e^{i\omega t} dt \\
 &= f(t) + g_r(t)
 \end{aligned} \tag{5-14}$$

where $g_r(t)$ is the transient response of the reflected signal due to the branch line.

If we move the source point and observation point away from the aperture ($p \neq 0$ and $z < 0$), we can still obtain the transient response. We define $\tilde{g}(t)$ as the time response for this case. Then $\tilde{g}(t)$ can easily be evaluated according to the time shifting property of the Fourier transform, if we have a known $g(t)$, viz:

$$\tilde{g}(t) = f\left(t - \frac{p+z}{v_c}\right) + g_r\left(t - \frac{p-z}{v_c}\right) \tag{5-15}$$

The difference between $g(t)$ and $\tilde{g}(t)$ is the time delay; therefore, it is not necessary to compute $\tilde{g}(t)$ for the general case.

5.4 Numerical Results

In this section, we present the numerical results of the transient response. We use the algorithm SIG (Lager and Azevedo, 1985) to compute the inverse Fourier transform and plot the curves.

Fig 5-3 shows the early time portion of the transient response of the reflected wave $g_r(\omega_c t)$ with the parameters $a = 1.5$, $d/a = 1.333$, and $c/a = 4.833$. It can be seen that $g_r(\omega_c t)$ rises and falls in synchronism with $f(\omega_c t)$ before a certain $\omega_c t$ is reached ($\omega_c t = 30$ radians in Fig 5-3). This means that there is no reflection when $\omega_c t < 30$ radians. But a discontinuity exists at this point. The time required for the wave to travel from the source to the bottom of the branch line and back is calculated to be $\omega_c t = 29.3$ radians. Therefore, the result from the figure matches the theoretical result. Another example is given in Fig 5-4. It shows a truncated $g_c(\omega_c t)$ with the parameters $a = 1.5$, $d/a = 1.333$, and $c/a = 24.0$. The theoretical calculation gives $\omega_c t = 150.72$ radians for these parameters and the reflection time obtained from the curve is about 150 radians.

The effects of the first higher order mode in the branch line can be seen in the transient response. When the incident impulse impinges on the bottom of the branch line, a portion of it is reflected. Meanwhile, amplitude oscillations occur which eventually damp to zero. In Fig 5-5, we employ the same parameters as in Fig 5-3. The interval between two ripples (when $\omega_c t > 120$ radians) in Fig 5-5 is about 8.28 radians, which corresponds to the first higher order cutoff frequency ($\omega/\omega_c = 0.75$) for this case; therefore, the ripples in Fig 5-5 are caused by the higher order mode. If we increase d/a , the interval between two ripples changes. Fig 5-6 shows $g_r(\omega_c t)$ with the same parameters as those of Fig 5-5, except $d/a = 2.666$.

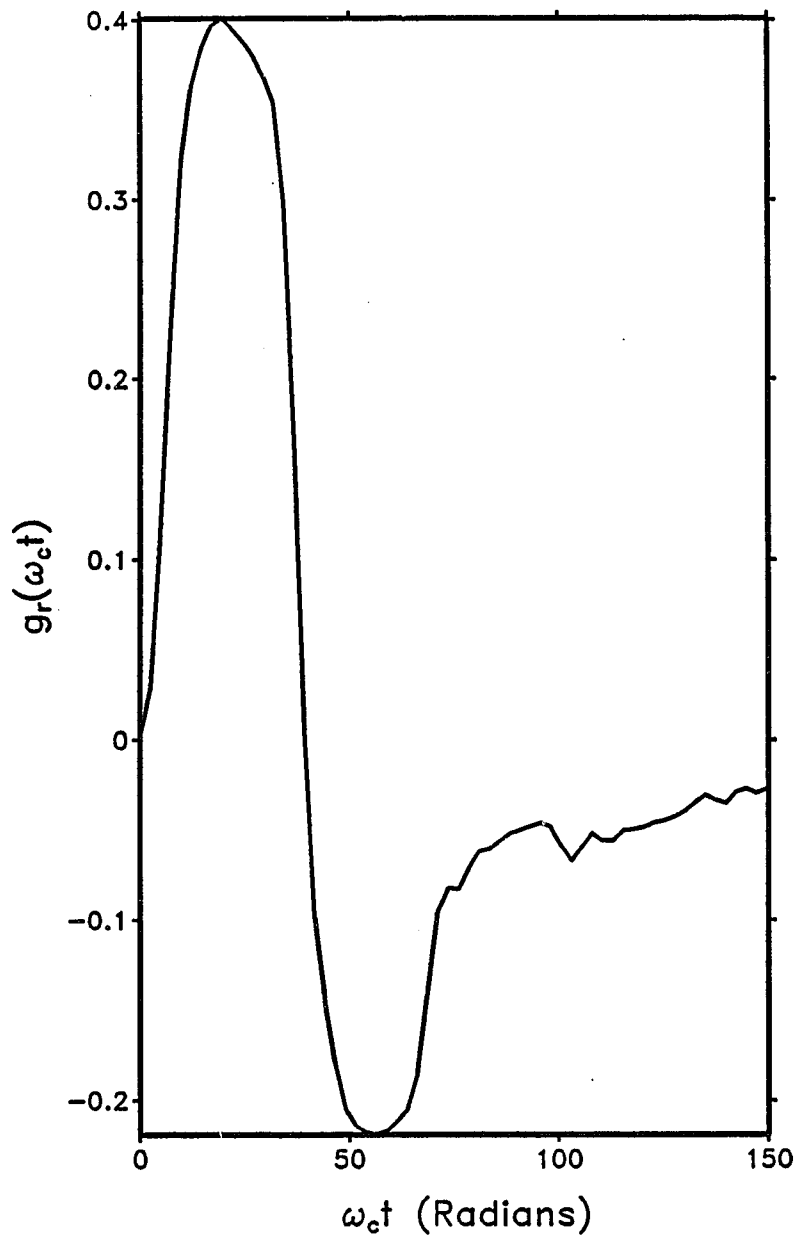


Figure 5-3 The transient response of the reflection coefficient $g_r(\omega_c t)$, where $a = 1.5$, $d/a = 1.333$, and $c/a = 4.833$. ($\omega_c = 6.28 \times 10^8$ radians/second)

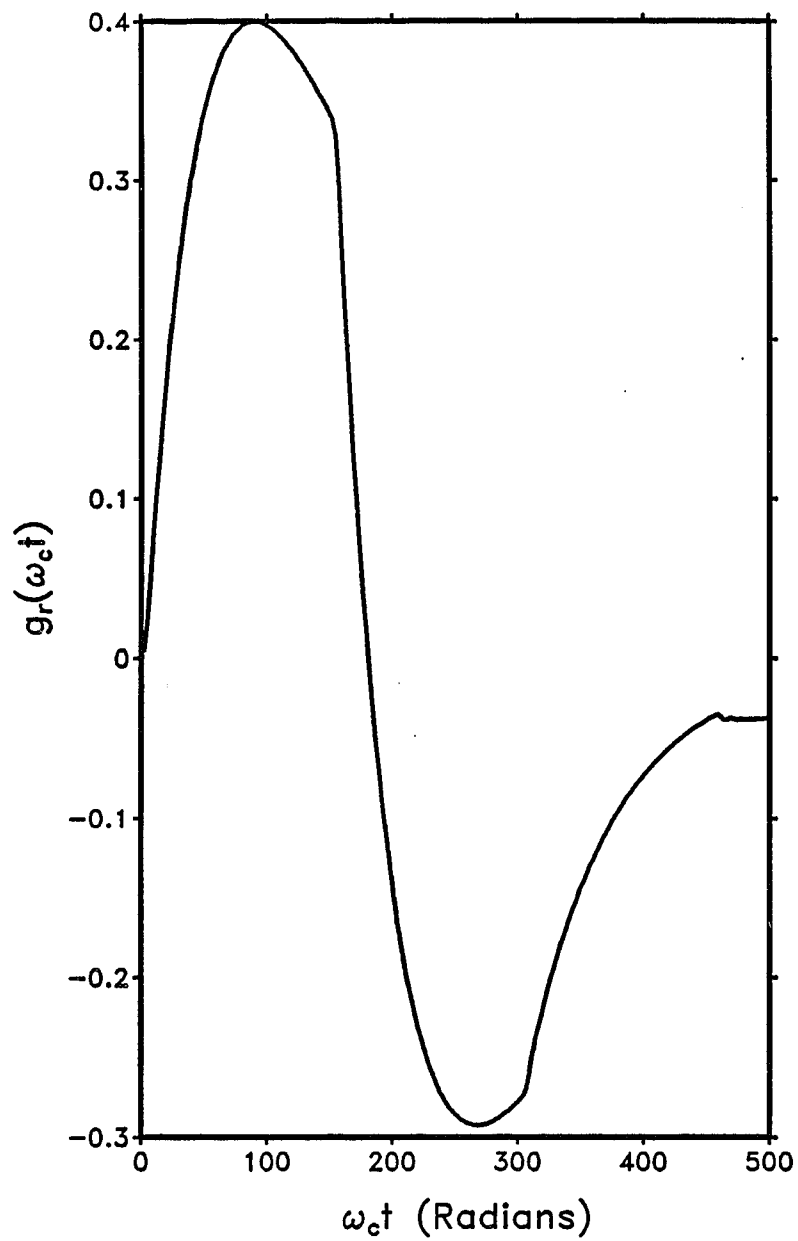


Figure 5-4 The transient response of the reflection coefficient $g_r(\omega_c t)$, where $a = 1.5$, $d/a = 1.333$, and $c/a = 24.0$. ($\omega_c = 6.28 \times 10^8$ radians/second)

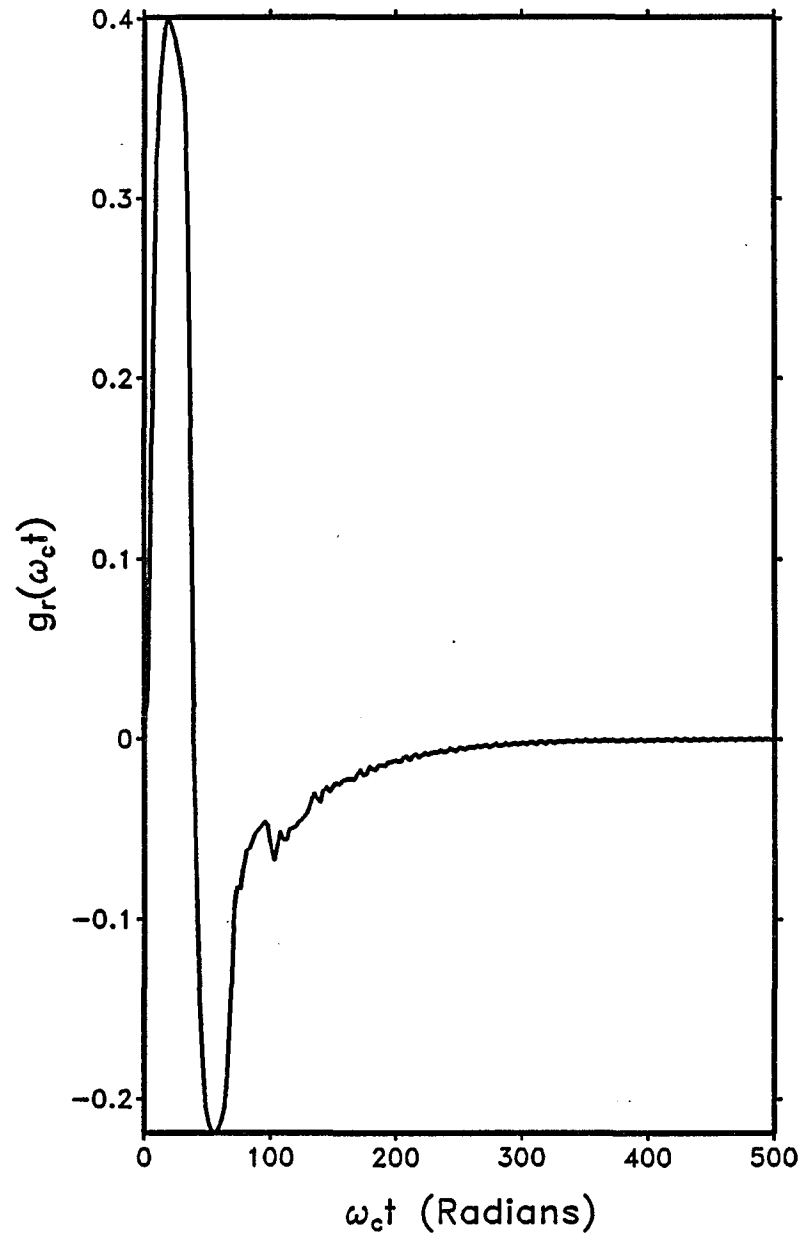


Figure 5-5 The transient response of the reflection coefficient $g_r(\omega_c t)$, where $a = 1.5$, $d/a = 1.333$, and $c/a = 4.833$. ($\omega_c = 6.28 \times 10^8$ radians/second)

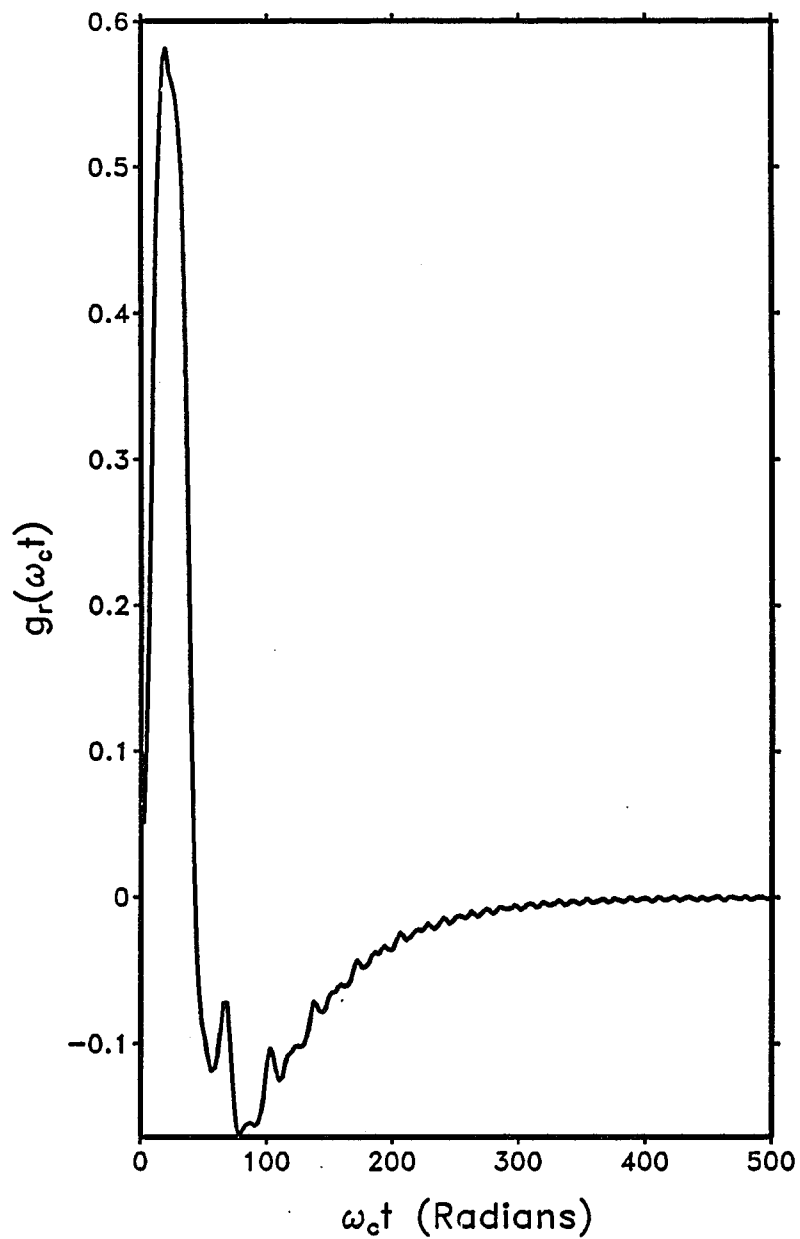


Figure 5-6 The transient response of the reflection coefficient $g_r(\omega_c t)$, where $a = 1.5$, $d/a = 2.666$, and $c/a = 4.833$. ($\omega_c = 6.28 \times 10^8$ radians/second)

The period between two ripples in Fig 5-6 must be double that of Fig 5-5, i.e. 16.70 radians. The intervals measured from the curve are about 17.14 radians, which correlates with the calculated value.

We next consider a case (Fig 5-7) where the higher order mode does not propagate until a frequency beyond where we have truncated the spectrum. However, small ripples are still present. We attribute these to truncation error. Indeed, let us increase the rise time and fall time of the double exponential function and see if the amplitudes of the ripples increase or decrease. Fig 5-8 shows $g_r(\omega_c t)$ whose parameters are the same as those for Fig 5-7 except for the rise time and fall time (rise time = $41.8ns$, fall time = $228ns$). It is obvious that the ripples have smaller amplitudes than the previous plots. Ideally, we would recover the signal in time domain undisturbed if the frequency spectra were of infinite bandwidth. However, this is impossible to achieve in practice. When we perform the numerical computation, we truncate $\Gamma(\omega)F(\omega)$ at 99 MHz. In fact, this procedure is similar to multiplying a window function $W(\omega)$ with $\Gamma(\omega)F(\omega)$. The window function behaves like a low pass filter. It will cut out the frequency components outside of the window. The counterpart to the frequency domain window function is the sinc function,

$$\text{sinc}(t) = \frac{\sin t}{t} \quad (5 - 16)$$

In time domain, the system response is the convolution of $g_r(t)$ with $\text{sinc}(t)$. The interval between the two nodes of $\text{sinc}(t)$ is $1/f_c$ ($10.1ns$ in our case). We count the intervals between two ripples and find that they are almost all similar and are approximately equal to $11.0ns$. Considering the sample errors and measurement errors, this value is close to the calculated result.

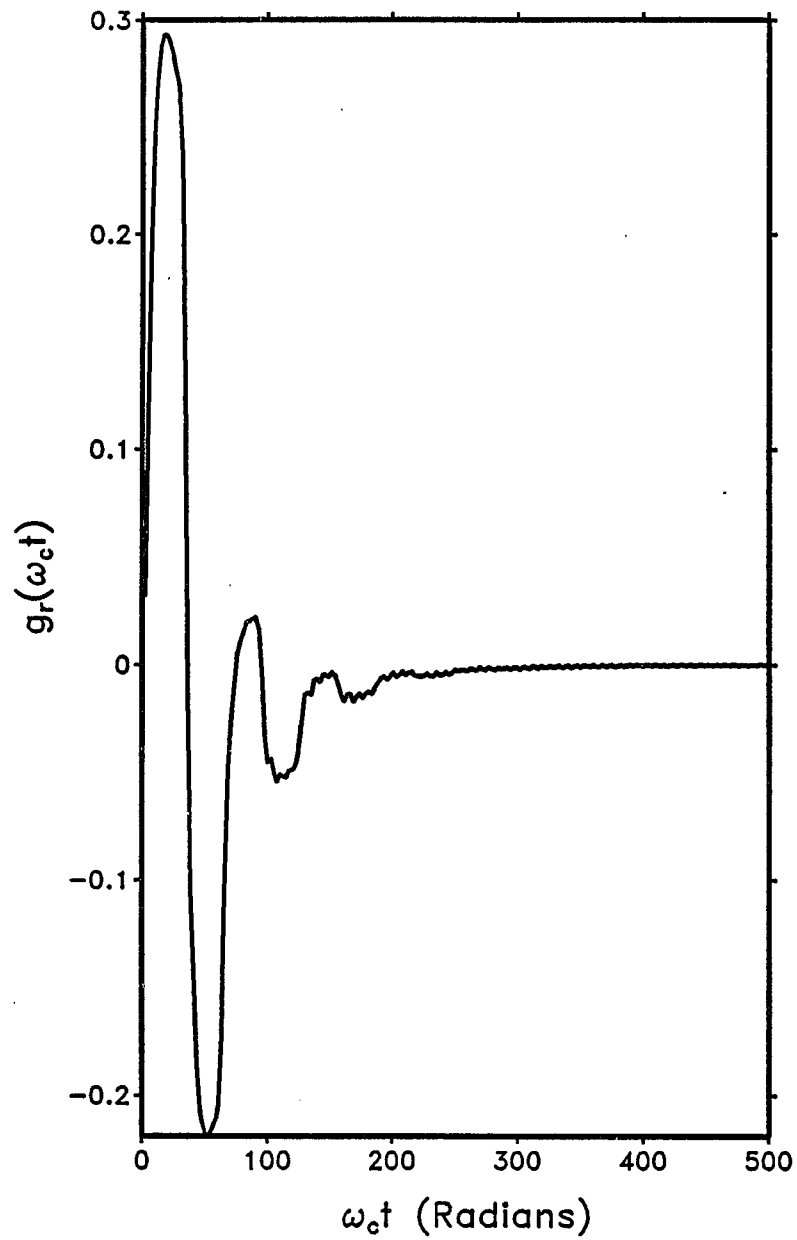


Figure 5-7 The transient response of the reflection coefficient $g_r(\omega_c t)$, where $a = 1.5$, $d/a = 0.833$, $c/a = 4.666$, rise time = $14.28ns$, and fall time = $134.12ns$. ($\omega_c = 6.28 \times 10^8$ radians/second)

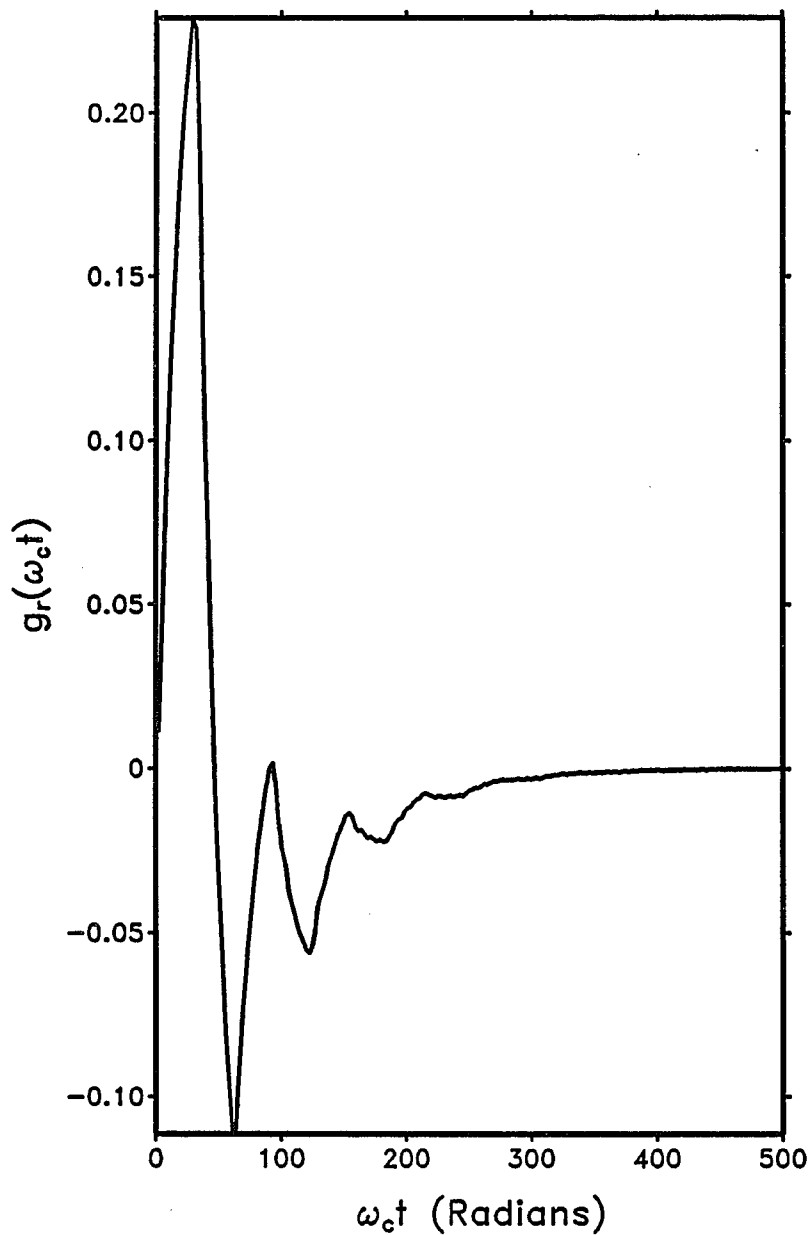


Figure 5-8 The transient response of the reflection coefficient $g_r(\omega_c t)$, where $a = 1.5$, $d/a = 0.833$, $c/a = 4.666$, rise time = $41.8ns$, and fall time = $228ns$. ($\omega_c = 6.28 \times 10^8$ radians/second)

Fig 5-9 shows plots of two curves: one is identical to Fig 5-4, and the other is for the case where $a = 1.5$, $d/a = 1.333$, and $c/a = 10$. Both curves have the same inputs. The difference between the two curves is that the discontinuity point of the slope takes place at different $\omega_c t$; the deeper the branch line, the longer the reflection time. The value of $\omega_c t$ at which the discontinuity occurs allows us to estimate the depth c . Fig 5-10 shows the transient response for a different width of the aperture but with the same branch line depth. It is clear that the reflections take place at the same time but that the peaks differ slightly due to the different amplitudes of the reflection coefficients in frequency domain.

Finally, we remark that there is one more waveform characteristic that allows us to estimate the parameter c . In Fig 5-7, note that the major feature of the waveform resembles a damped sinusoid. The sinusoidal appearing oscillation has a period of 58.34 radians or $\omega/\omega_c = 0.107$. This frequency corresponds to $c/\lambda = 0.25$, and we can obtain an estimate of c therefrom.

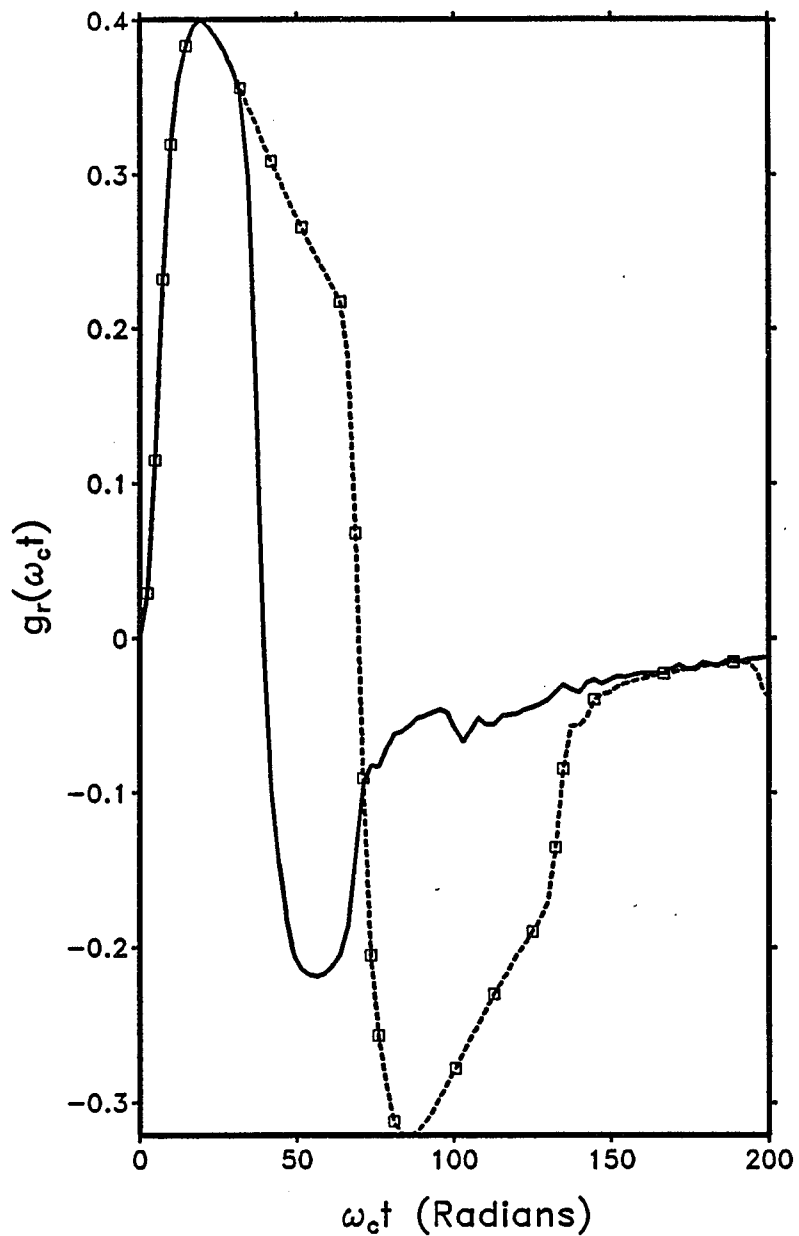


Figure 5-9 The solid line denotes $g_r(\omega_c t)$ with the parameters $a = 1.5$, $d/a = 1.333$, and $c/a = 4.833$. The dashed line with \square denotes $g_r(\omega_c t)$, with the parameters $a = 1.5$, $d/a = 1.333$, and $c/a = 10.0$. ($\omega_c = 6.28 \times 10^8$ radians/second)

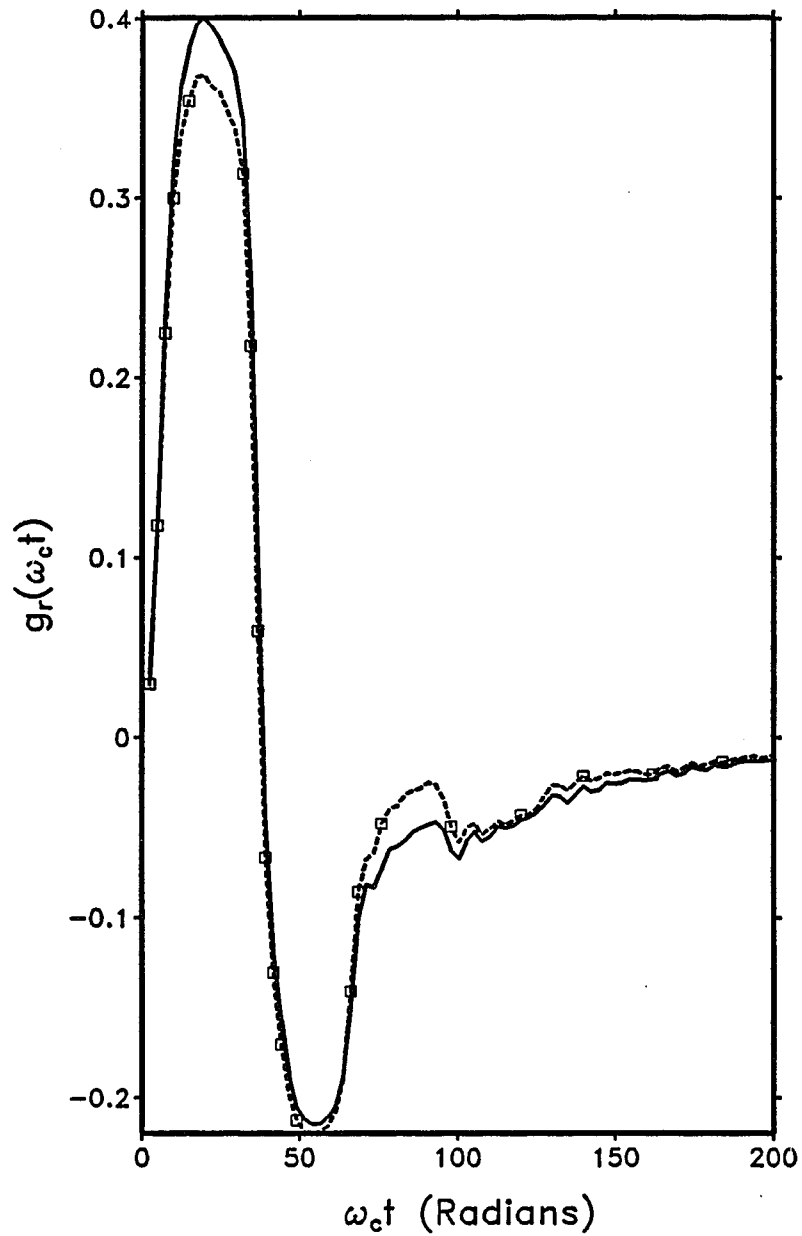


Figure 5-10 The solid line denotes $g_r(\omega_c t)$ with the parameters $a = 1.5$, $d/a = 1.333$, and $c/a = 4.666$. The dashed line with \square denotes $g_r(\omega_c t)$, with the parameters $a = 1.5$, $d/a = 1.166$, and $c/a = 4.666$. ($\omega_c = 6.28 \times 10^8$ radians/second)

CHAPTER 6

CONCLUSIONS AND RECOMMENDATIONS

The transient scattered fields from a junction between a parallel-plate waveguide and a branch line have been determined when a TEM wave impinges on the junction. Our task can be divided into roughly two parts. The first part is the determination of the reflected wave in the frequency domain by solution of an integral equation at the aperture. This includes the derivation of the TM mode equations from Maxwell's equations, the formulation of the field expressions in the structure by means of the Green's function, and the establishment of the integral equation by imposing boundary conditions. The solution of the integral equation is achieved by means of two approaches, namely, the method of moments (MOM) and the low frequency approximation. The second part of this work involves the determination of the transient scattered field response in the waveguide by using the Fourier transform method. The transient response provides enough information to estimate the depth and the width of the branch line as well as its position for a parametric inverse experiment, where the scatterer can be described by input and output data.

It was necessary to study the singularities of the Green's functions and the singularities at the edges of the structure before we started the numerical work. This study led us to properly choose the expansion function and the point testing function so that those singularities are overcome when performing computational work. In addition, speeding the convergence of the summations in every matrix element is very important for our work to be successful. For example, to compute

the frequency-domain response using a 40×40 matrix with the asymptotic terms may take about 20 minutes of CPU time. We have not tried to compute a 40×40 matrix without the asymptotic terms, but an average of 2 hours of CPU time is required to directly sum 100,000 terms in a single summation (see Table 4-1 and Table 4-2). Since there are 6 summations per matrix element, about 20,000 hours (over two years) of CPU time would be required to compute the matrix.

Having seen the accuracy of the mathematical model in predicting the characteristics of the simulator, we could use these results as a starting point in analysing more complicated systems that occur in practice. An example would be the case where the waveguide and branch line have different permittivities, permeabilities, and conductivities. In this situation, the singularities caused by the edges would differ from our problem. It would also be possible to expand the model to include several branch lines of varying sizes at different positions in the waveguide. This would be more representative of actual geophysical well logging where there may be several bed boundaries and intrusions of varying sizes and chemical composition. Such a situation would be more difficult to analyse because the reflected waves themselves impinge on the discontinuities causing multiple reflections and coupling between branch lines.

- Marcuvitz, N., Ed., (1951) Waveguide Handbook, McGraw-Hill Book Company, Inc., New York.
- Mitra, R., Ed., (1973), Computer Techniques for Electromagnetics, Pergamon Press, New York.
- Mitra, R. and S. W. Lee (1971), Analytical Techniques in the Theory of Guided Waves, MacMillan Company, New York.
- Shen, H. M., R. W. P. King and T. T. Wu (1983), "An Experimental Investigation of the Parallel-Plate EMP Simulator with Single-Pulse Excitation", IEEE Trans. EMC-25, 358-366.
- Shen, L. C. and J. A. Kong (1983), Applied Electromagnetism, Brooks/Cole Engineering Division, Monterey.
- Stakgold, I. (1979), Green's functions and Boundary Value Problems, John Wiley & Sons, New York.
- Wait, J. R. (1982), Geo-Electromagnetism, Academic Press, New York.
- Wait, J. R. (1986), "Propagation Effects for Electromagnetic Pulse Transmission," Proc. IEEE 74, to appear.